DOT/FAA/AR-04/40,P3

Office of Aviation Research
Washington, D.C. 20591

Explicit Finite Element Modeling of Multilayer Composite Fabric for Gas Turbine Engine Containment Systems

Part 3: Model Development and Simulation of Experiments

November 2004

Final Report

This document is available to the U.S. public through the National Technical Information Service (NTIS), Springfield, Virginia 22161.

U.S. Department of Transportation
Federal Aviation Administration

NOTICE

Technical Report Documentation Page

1. Report No.	2. Government Accession No.	3. Recipient's Catalog No.
DOT/FAA/AR-04/40,P3		

4. Title and Subtitle	5. Report Date
EXPLICIT FINITE ELEMENT MODELING OF MULTILAYER COMPOSITE FABRIC FOR GAS TURBINE ENGINE CONTAINMENT SYSTEMS PART 3: MODEL DEVELOPMENT AND SIMULATION OF EXPERIMENTS	November 2004
	6. Performing Organization Code

7. Author(s)	8. Performing Organization Report No.
Jeffrey Simmons, David Erlich, and Donald Shockey	

9. Performing Organization Name and Address	10. Work Unit No. (TRAIS)
SRI International 33 Ravenswood Avenue Menlo Park, CA 94025	11. Contract or Grant No. 01-C-AW-ASU

12. Sponsoring Agency Name and Address	13. Type of Report and Period Covered
U.S. Department of Transportation Federal Aviation Administration Office of Aviation Research Washington, DC 20591	Final Report 8/2001 – 5/2003
	14. Sponsoring Agency Code ANE-100, ANM-100

15. Supplementary Notes

The FAA William J. Hughes Technical Center COTR was Donald Altobelli.

16. Abstract

Under the Federal Aviation Administration Airworthiness Assurance Center of Excellence and with support from the Aircraft Catastrophic Failure Prevention Program, SRI International collaborated with Arizona State University; Honeywell Engines, Systems and Services; and the National Aeronautics and Space Administration Glenn Research Center to develop a computational model for designing and evaluating ballistic fabric containment structures. This report describes the model and compares the results of static and impact penetration tests with the results of computational simulations.

17. Key Words	18. Distribution Statement
Fan containment, Jet engine, Composite fabric, Ballistic impact, Zylon, Kevlar	This document is available to the public through the National Technical Information Service (NTIS) Springfield, Virginia 22161.

19. Security Classif. (of this report)	20. Security Classif. (of this page)	21. No. of Pages	22. Price
Unclassified	Unclassified	59	

TABLE OF CONTENTS

LIST OF FIGURES

LIST OF TABLES

LIST OF ACRONYMS

ACFPP	Aircraft Catastrophic Failure Prevention Program
ASU	Arizona State University
FAA	Federal Aviation Administration
LSTC	Livermore Software Technology Company
NASA GRC	National Aeronautics and Space Administration Glenn Research Center
SRI	SRI International

EXECUTIVE SUMMARY

Modeling a multilayer fabric composite for engine containment systems during a fan blade-out event has been a challenging task. Nonlinear transient (explicit) finite element (FE) analysis has the greatest potential of any numerical approach available to industry for analysis of these events. Significant research is still required to overcome difficulties with numerical stability, material modeling (pre- and postfailure), and standardizing model methods to achieve accurate simulation of the complex interactions between individual components during these high-speed events. The primary focus of this research was to develop the methodology for testing, modeling, and analyzing a typical fan blade-out event in a multilayer fiber fabric composite containment system. ABAQUS FE code was used to verify the basic material model (prefailure state) developed through laboratory testing. LS-DYNA was the primary modeling tool used in the explicit FE analysis of ballistic events.

During the Fourth Federal Aviation Administration (FAA) Uncontained Engine Debris Characterization Modeling and Mitigation Workshop (held in May 2000 at SRI International, Menlo Park, CA), a representative of Honeywell Engines, Systems & Services presented the capability of modeling complicated engine hub-burst and fan blade-out events. Predicting most of the event with high confidence was shown. At the same time, SRI presented their efforts on modeling the material characteristics within LS-DYNA and developing a new composite fiber material called Zylon® that appeared to be stronger, lighter, and more temperature-resistant than Kevlar®. Both parties showed interest in each other's work, and both agreed they could benefit from each other if collaborative mechanisms could be arranged. After the workshop, Honeywell and SRI contacted each other and began talks of a joint project. The FAA, the National Aeronautics and Space Administration (NASA) Glenn Research Center (GRC), and Arizona State University (ASU) were later invited into the discussion, resulting in this FAA-funded research under the Aircraft Catastrophic Prevention Program and the Airworthiness Assurance Center of Excellence Program.

The goal of this research, was to use the technical strengths of Honeywell, SRI, NASA GRC, and ASU for developing a robust explicit FE analysis modeling methodology for the purposes mentioned above. Since the development of an experimental set of data to support the calibration of the FE models is essential, various experimental methods to measure material and structural response of the fabrics were conducted. NASA GRC, under the NASA Aviation Safety Program, conducted a series of fabric engine containment ring tests that were used for modeling in this program.

Each member of the team took a leadership role and developed a comprehensive report describing the details of the research task and the findings. The complete FAA report is comprised of the following four separate reports (parts 1 through 4).

- Part 1: Static Tests and Modeling by Arizona State University Department of Civil Engineering

- Part 2: Ballistic Testing by NASA Glenn Research Center

- Part 3: Material Model Development and Simulation of Experiments by SRI International

- Part 4: Model Simulation for Ballistic Tests, Engine Fan Blade-Out, and Generic Engine by Honeywell Engines, Systems & Services

SRI's role was to produce a FE model for multilayer fabric, implement the model into LS-DYNA, determine material properties for Zylon and Kevlar from static tests, and evaluate the model by simulating fragment impact experiments. This report describes the model development and the results of the computational simulations.

The form of the fabric model and the material parameters were based on observations and measurements from uniaxial and cyclic load experiments on single plies of fabric performed at ASU and SRI. Multiple fabric plies were modeled with one shell element, whose thickness was proportional to the number of plies. A single set of material constants was determined for each fabric.

Additional experiments were performed in which a fragment simulator penetrated multiple layers of fabric wrapped around a steel ring, a configuration representative of an engine containment ring. Quasi-static tests were performed at ASU, and ballistic tests were performed at NASA GRC. The model was evaluated by simulating these tests.

Overall, the simulation results agreed well with test results. For the quasi-static tests on Kevlar, the calculated values for peak load and strain to failure were close to the measured average values. For Zylon, the calculated peak load was about 15% below the measured average for the quasi-static tests.

For the ballistic tests on Kevlar, the model closely predicted the energy absorbed for the 4-, 8-, 16- and 24-ply tests, but underpredicted the energy absorbed for the 1- and 2-ply tests. For Zylon, the model predicted the energy-absorbed values within the test data scatter for 4, 8, and 16 layers, but underpredicted the energy absorbed for 24 plies.

The results showed that the choice of analysis parameters and solution algorithms (particularly the choice of slideline parameters) has a big effect on the energy absorbed that was calculated in ballistic tests. Future work will need to determine the sensitivity of the model to these parameters. An improved treatment of rate effects is also needed. In addition, a procedure for using multiple layers of shell elements to model many fabric plies will facilitate design computations.

1. INTRODUCTION.

1.1 PURPOSE.

This research effort was undertaken as a direct result of discussions from the Fourth Federal Aviation Administration (FAA) Uncontained Debris Characterization Modeling and Mitigation Workshop (held in May 2000 at SRI International). A teaming effort between government, academia, and industry was seen as an excellent opportunity to transition fabric modeling and testing research, that was being sponsored by the FAA Aircraft Catastrophic Failure Prevention Program (ACFPP), into commercial aircraft.

1.2 BACKGROUND.

Over the last 7 years, under the sponsorship of the ACFPP of the FAA, SRI conducted a research program aimed at enhancing the safety of civilian air travel by reducing the likelihood of a catastrophic accident in the event of an uncontained engine failure.

SRI began by reviewing advanced military armor technology to identify materials, armor structures, and projectile defeat concepts that could be used in designing barriers to turbine engine fragments for commercial aircraft. Experiments and computations were then performed to evaluate these findings. The work identified an advanced material with significantly better resistance to fragment penetration, demonstrated barrier structures that can protect against small to medium turbine engine blade fragments at a tenth of the weight of aluminum barriers, and developed a computational capability for designing fragment barriers. Full-scale ballistic experiments on fuselage sections with advanced polymer fabric barriers confirmed the ballistic effectiveness of lightweight fabric barriers.

The results attracted the attention of the commercial aircraft industry. Under continued sponsorship by the ACFPP and new grants from the Airworthiness Assurance Center of Excellence (AACE), SRI worked with an aircraft engine manufacturer and an airframe manufacturer to transfer this technology to industry and to address specific needs of the aircraft industry. This project with Arizona State University (ASU), Honeywell Engines, Systems & Services, and National Aeronautics and Space Administration (NASA) Glenn Research Center (GRC) aimed at adapting the SRI fabric model to address fragment containment issues, while another project with the University of California at Berkeley and The Boeing Company evaluated the effectiveness of multilayer Zylon® fabric in protecting fuselage structures from uncontained debris.

SRI's effort in the ASU, Honeywell, and NASA GRC program is presented here. The objective of this research was to develop and demonstrate a computational model of ballistic response of fabrics under engine containment conditions. The desired end product was a computational capability for designing multilayer fabric engine containment structures for commercial transport aircraft. SRI's part was (1) to perform static laboratory experiments (swath tests) to measure response of multilayer fabrics to slow penetration, (2) to use the data and observations along with ring test data from ASU and ballistic data from NASA GRC to develop a computational model of fabric response, and (3) to evaluate the model by simulating the experiments and comparing

computed and observed behavior. The procedures and results of this effort are presented in the following sections.

2. FINITE ELEMENT ANALYSIS.

2.1 BACKGROUND.

A computational model is being developed that can be used as a design tool for choosing or evaluating parameters for fragment barriers containing ballistic fabric. The design model, implemented into the LS-DYNA finite element code, uses shell elements with an orthotropic continuum formulation to model the fabric. Because calculations run relatively quickly (about 15 minutes using a four-processor Pentium III Linux cluster for a 20,000 element simulation of a gas gun experiment), the model allows design parameters to be varied and evaluated. The response of barrier characteristics, such as size of fabric, gripping conditions, number of fabric plies, and yarn pitch, can be simulated as well as the size, orientation, and velocity of a fragment. Thus, the model is intended to be useful in designing and certifying fragment barriers, i.e., in determining how many plies of woven fabric are needed to stop a given fragment threat and in computing the loads applied to the supporting structure. The physical properties of the ballistic fabrics used in this program, Zylon AS® and Kevlar 49®, are listed in table 1.

TABLE 1. PROPERTIES OF ZYLON AND KEVLAR FABRICS

Trade Name		Zylon AS	Kevlar 49
Material		Poly-benzobisoxazole	P-Aramid
Volume Density (from manufacturer)	(g/cm^3)	1.54	1.44
Yarn Denier—As-Ordered	(g/9 km)	500	1420
Yarn Denier—Measured	(g/9 km)	500	1490
Yarn Linear Density—Measured	(mg/cm)	0.556	1.656
Yarn Cross-Sectional Area	(cm^2 x 10^{-4}) (in^2 x 10^{-5})	3.61 5.59	11.50 17.82
Yarn Count	(yarns/cm)	35 x 35	17 x 17
Fabric Ply thickness (approx.)	(in.) (mm)	0.008 0.21	0.011 0.28
Fabric Areal Density—Measured	(g/cm^2) (lb/ft^2)	0.01575 0.0323	0.02275 0.0466

2.2 THE FINITE ELEMENT MODEL FOR BALLISTIC FABRIC.

2.2.1 Fabric Response in Uniaxial Tension.

The response of a single ply of Kevlar® fabric tested in uniaxial tension, shown in figure 1, is representative of ballistic fabric, and has the following features: (1) a low initial modulus due to straightening of yarn crimp, followed by (2) a linear response up to initial damage (breaking of

fibers), which results in (3) a reduced and nonlinear modulus up to a peak loading, followed by (4) a postpeak drop in strength with increased strain.

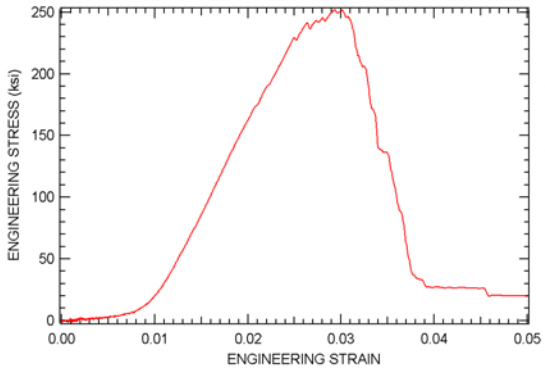

FIGURE 1. RESPONSE OF KEVLAR FABRIC TO UNIAXIAL TENSION LOADING

2.2.2 Fabric Response Under Cyclic Loading.

The cyclic response of ballistic fabric in tension is shown in figure 2. Zylon (figure 2(a)) and Kevlar (figure 2(b)) show a similar response. Unloading and subsequent reloading of the fabric follow a single curve that is nearly linear with a modulus that is stiffer than the original loading modulus for unloading before the peak stress is reached. As the fabric acquires damage, the unloading modulus decreases.

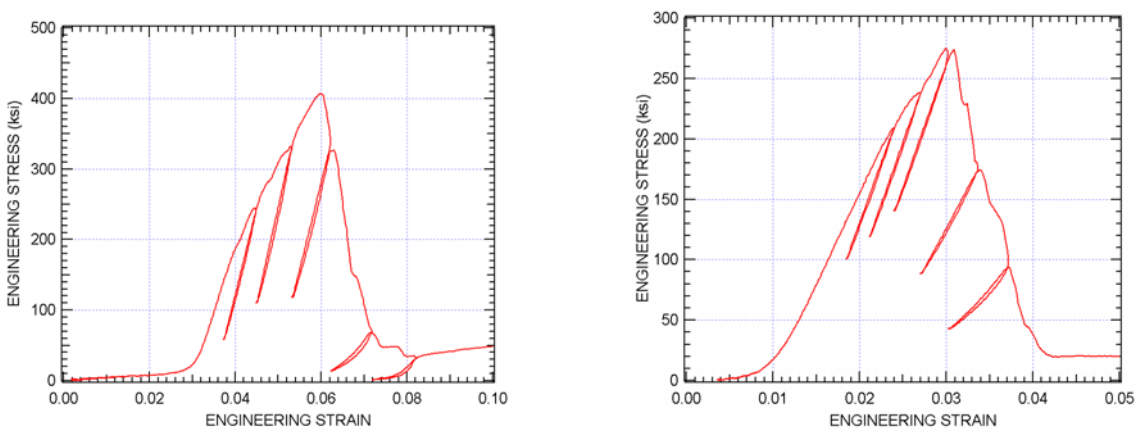

(a) Zylon (b) Kevlar

FIGURE 2. CYCLIC RESPONSE OF FABRIC TO UNIAXIAL TENSION

2.2.3 Model Basics.

The ballistic fabric model being developed is an orthotropic model with a stress-strain response for each of the two yarn (local x and y) directions. The stress-strain responses in the two directions are assumed to be uncoupled, that is, the interaction between the orthogonal yarns due to the weave pattern is ignored. However, the failure response is coupled.

2.2.4 Damage Mechanics.

The approach to modeling the response of ballistic fabric was to combine a mechanistic constitutive law for the fibers in the yarns in each direction with a damage law that governs fiber breakage.

Figure 3 shows the stress-strain curve for a fiber in a yarn for cyclic loading. Cyclic loading is important because it gives data in the amount of fabric damage that has been experienced in the loading process. Initially, the fiber has a low modulus corresponding to the stress required to straighten the crimp in the yarn. Once the fiber is straightened, the response in loading is linear elastic up to a peak stress at which failure occurs, i.e., the fibers begin to break. On unloading and subsequent reloading, the fiber is linear elastic with a modulus twice as stiff as the original elastic modulus. It is believed that the change in modulus on unloading and subsequent hysteresis corresponds to the rearrangement of yarns in the fabric. These effects may depend on fabric weave or yarn twist, but this dependence was not investigated. In compression, the model fiber has a very small (but nonzero) modulus.

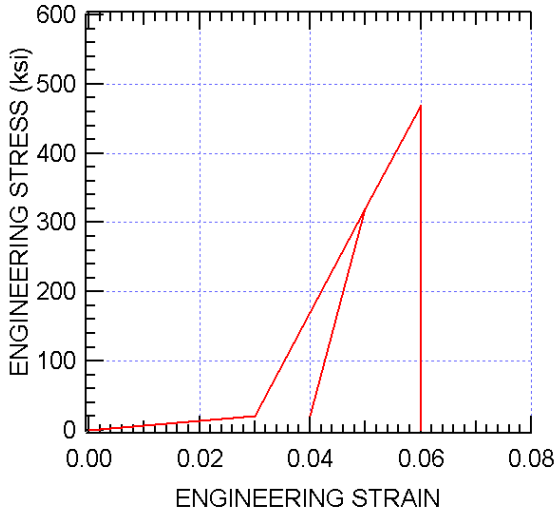

FIGURE 3. STRESS-STRAIN CURVE FOR A FIBER

To model damage and failure for the fabric, the mechanism of tensile failure of the fibers in the yarn was considered. Each yarn is typically made up of 200 to 250 fibers. As shown in figure 3, the fibers are assumed to be elastic until they break in tension. For the continuum model, the axial stress in the fabric, σ_a, is assumed to be the stress from the strain in the unbroken yarns. Under monotonic loading, the axial stress is given by

$$\sigma_a = E\tilde{\varepsilon}_a\left(1 - d_\sigma\right) \tag{1}$$

where, E is the fiber axial modulus, d_σ is the fraction of broken yarns (which varies from zero to one), and $\tilde{\varepsilon}_a$ is the effective axial strain defined as the total axial strain, ε_a, minus the crimp strain, ε_{cr}. For a dynamic analysis, the rate of axial stress, $\dot{\sigma}_a$, is given by

$$\dot{\sigma}_a = E(1-d_\sigma)\dot{\tilde{\varepsilon}}_a - E\dot{d}_\sigma\tilde{\varepsilon}_a \tag{2}$$

It is assumed that the fibers do not all break at the same time, but because of imperfections in the fibers and differences in fiber stresses due to misalignment or different prestrain, the fibers break over some range of stress and strain. The fiber breakage is assumed to be a function of fiber stress, f, as shown in figure 4, namely, that at some minimum value of stress, $f_{\min}$, fibers start to break. Damage is assumed linear with fiber stress up to f_{peak}, the point of peak axial stress, $\sigma_{\max}$, and then damage accumulates exponentially, as the fiber stress approaches the stress at which all the fibers are broken, f_f.

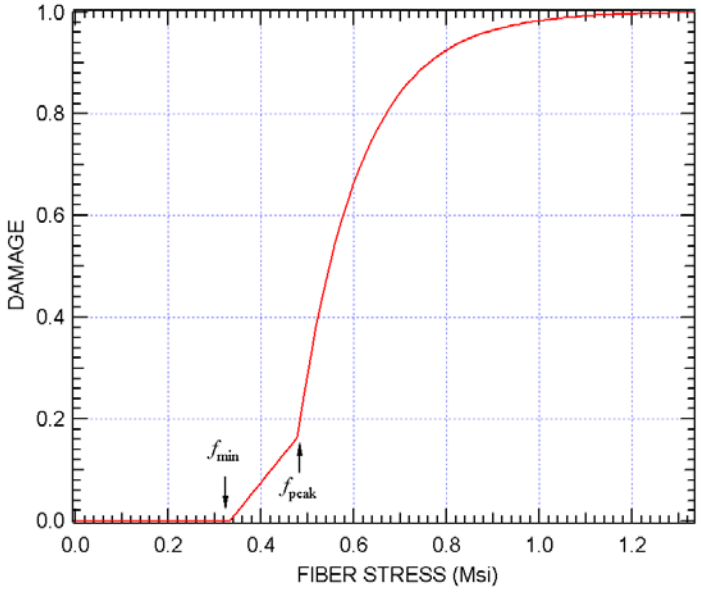

FIGURE 4. FIBER DAMAGE AS A FUNCTION OF STRAIN

2.2.5 Rate Dependence for Failure.

The model has a rate dependency in the damage formulation that incorporates a time constant, t_c, that corresponds to the time it takes fibers to break. Incremental damage to the fibers during a time step is calculated as

$$\Delta d = (d_\sigma - d_0)\left(1 - e^{-\frac{\Delta t}{t_c}}\right) \tag{3}$$

where d_0 is the level of damage at the beginning of the time step, and d_σ is the damage level based on the current stress state (given in equation 3). This form of rate dependence helps to prevent a sharp short-duration load spike (such as those experienced in initial impact for the slideline formulation) from instantaneously failing the fabric.

In incremental form, equation 4 is given by

$$\Delta\sigma_a = E(1-d)\dot{\tilde{\varepsilon}}_a \Delta t - E\Delta d\tilde{\varepsilon}_a \tag{4}$$

where Δt is the computational time step.

For numerical stability, the increase in damage Δd at any computational step is limited to a small number, e.g., 0.002. When all the fibers are broken (i.e., the damage equals one), the element is removed from the calculation (eroded).

2.2.6 Model Response.

Combining the stress-strain response for a fiber (figure 3) with the damage law shown in figure 4 gives a calculated stress-strain response for fabric under cyclic load, as shown in figure 5. The behavior predicted by the model agrees very well with the test results over the entire range of strain. The peak stress, the softening portion of the curve, and the unloading and reloading cycles are consistent.

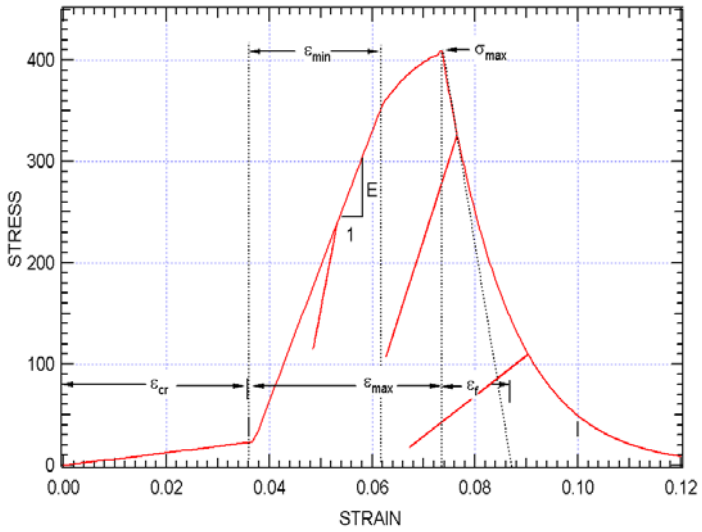

FIGURE 5. UNIAXIAL STRESS-STRAIN CURVE FOR BALLISTIC FABRIC MODEL

2.2.7 Off-Diagonal and Shear Response.

Values for other moduli such as shear modulus, G, compression modulus, or crimp modulus are assumed to be linear elastic with values that should be very small compared with the modulus in tension. However, if these moduli are chosen as zero, the simulation typically crashes due to

numerical problems. Therefore, the values for these moduli are set to 0.5% of the tensile modulus. Thus, the constitutive relations for the fabric material in the shell elements are given by

$$\begin{aligned} \sigma_{xx} &= f(\varepsilon_{xx})d \\ \sigma_{yy} &= f(\varepsilon_{yy})d \\ \sigma_{zz} &= 0 \\ \tau_{xy} &= G\,\varepsilon_{xy} \\ \tau_{yz} &= G\,\varepsilon_{yz} \\ \tau_{zx} &= G\,\varepsilon_{zx} \end{aligned} \tag{5}$$

2.2.8 Multiple Plies.

Static ring tests were performed at ASU in which an impactor was pushed through multiple layers of fabric wrapped around a 32-inch-diameter steel ring. Multiple layers of fabric ranging from 1 to 24 plies were tested. The impactor force and displacement were measured. The results are shown in figure 6(a) for Kevlar and in figure 6(b) Zylon in terms of force and ply as a function of impactor displacement. The curves were realigned slightly to lineup at approximately 800 pounds force to allow for the differences in initial slack in the test fixture. The bumps in the curves at low displacement are due to clamping of the fabric in the test setup. Except for the two 24-ply tests, the ASU ring test results show very little difference in force-displacement for multiple plies of fabric, i.e., the force to displace eight layers of fabric is simply eight times the force for a single layer. The characteristic of the curve for 24 layers of Kevlar, namely, a lower stiffness and peak stress and larger strain to peak and strain to failure, is characteristic of the layers having nonuniform pre-tension. Likewise, 24 layers of Zylon had lower force and ply than the tests with fewer plies.

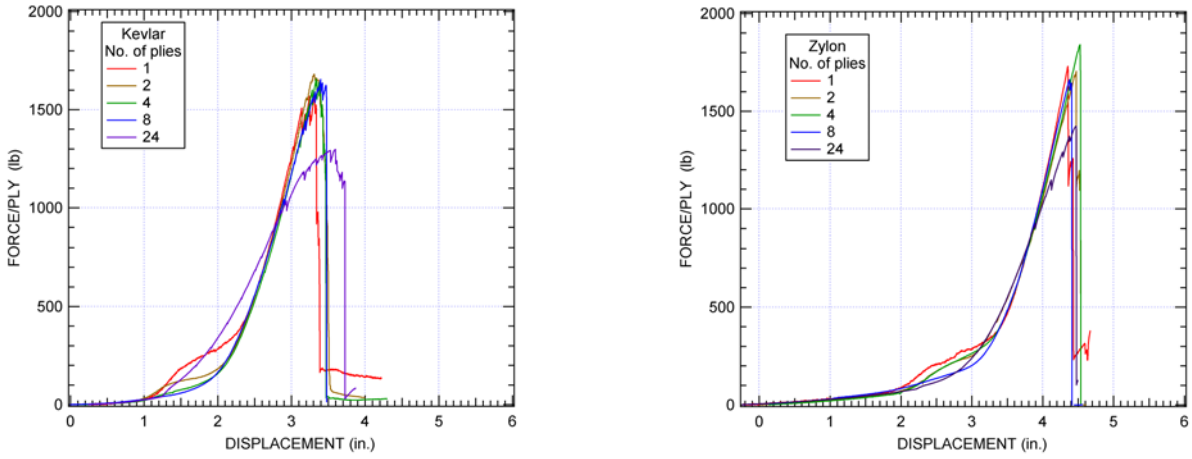

(a) Kevlar (b) Zylon

FIGURE 6. STATIC RING TEST RESULTS

Based on these results, multiple plies of ballistic fabric were modeled by simply increasing the thickness of the shell element by a factor equal to the number of plies. Because the fabric model uses shell elements with single-point integration, the element responds like a membrane, i.e.,

bending stiffness is negligible, and thus, the nonlinear increase in the bending stiffness with increased element thickness is not a problem. This model assumes that, for a multiple-ply target, the fabric yarns are all aligned in the same direction (e.g., 0° and 90°).

2.2.9 Fabric Slack.

The effect of fabric slack, which is due to lack of pre-tension in attaching the fabric (as opposed to yarn crimp, which is the waviness of the yarn due to the weaving process), can be modeled by adding an equivalent strain due to slack to the crimp strain. The effect of slack is to allow an initial strain to occur in the fabric without significant stress developing. It should be noted that fabric slack was not measured or modeled in this program.

2.3 ANALYSIS CONSIDERATIONS.

2.3.1 Mesh Size.

The finite element analyses were performed using LS-DYNA (beta Version MPP970 revision 1405). For this investigation, the mesh size of the fabric elements, 1/4-inch square, was dictated by Honeywell. This is an element size that is small enough to give reasonable resolution of stresses, but large enough that full engine simulations can be completed in a reasonable time.

2.3.2 Contact Parameters.

Simulations performed on this project have shown that the penetration response of the fabric can be strongly affected by choices of contact formulation and contact parameters. Details on these differences can be found in Honeywell's project report [1]. It was found that the best choice of contact algorithm was to use, in keyword format

*CONTACT_AUTOMATIC_SURFACE_TO_SURFACE

with segment-checking for interpenetration (the parameter soft set equal to 2). All other contact parameters were set equal to the default values.

2.4 APPROACH FOR MODEL DEVELOPMENT.

The approach for material model development for Zylon and Kevlar was to derive material parameters from simple single-ply uniaxial stress tests, and then verify the model by simulating the ASU quasi-static ring tests and the NASA ballistic impact tests.

2.5 SINGLE-PLY, QUASI-STATIC UNIAXIAL TESTS.

Single-ply uniaxial stress tests were performed at SRI and at ASU on both Zylon and Kevlar. The tests at SRI, which are described in this report, were performed by pushing an impactor transversely against a 10-inch-long swath of fabric that was held at both ends. The tests at ASU, described in reference 2, were performed by gripping and pulling in-plane 12-inch-long, 2.5-inch-wide swaths of fabric.

The results of these tests are shown in figure 7, along with the stress-strain response of a single-element model. The lower peak stresses for the Kevlar tests performed at SRI may be due to failure of the yarns at the grips. Material properties for the Kevlar and Zylon model are listed in table 1. The meaning of the parameters is explained in appendix A. Note that the material constants listed in table 2 are appropriate for this size mesh.

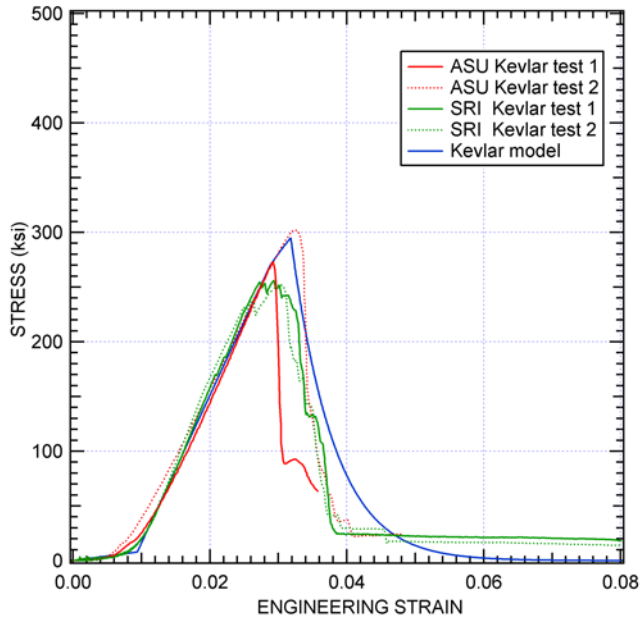

(a) Kevlar

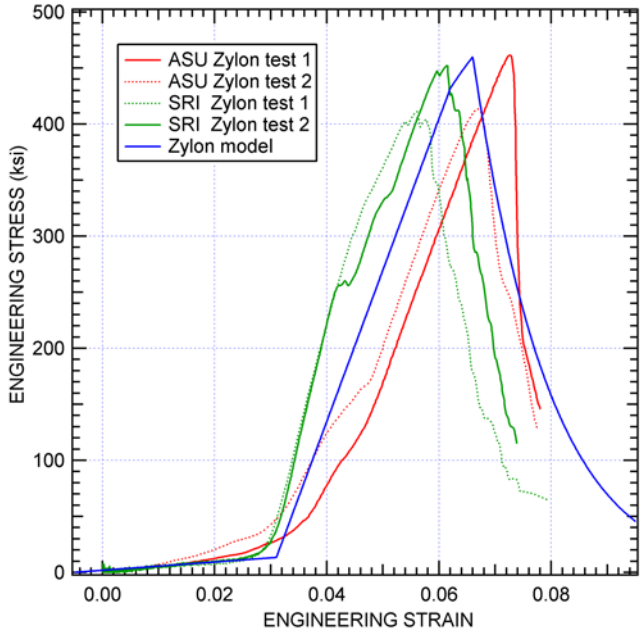

(b) Zylon

FIGURE 7. FABRIC MODEL FOR UNIAXIAL TESTS

TABLE 2. CONSTANTS FOR KEVLAR AND ZYLON

Name	Symbol	Kevlar 49	Zylon
Tensile Modulus	E	10.2 Msi (70.3 GPa)	13.3 Msi (91.7 GPa)
Peak stress	σ_{max}	0.305 Msi (2.10 GPa)	0.421 Msi (2.90 GPa)
Initial damage strain	ε_{min}	0.0235	0.025
Strain at peak stress	ε_{max}	0.0262	0.036
Crimp strain x direction	ε_{crx}	0.01	0.037
Crimp strain y direction	ε_{cry}	0.01	0.006
Failure strain	ε_{fail}	0.010	0.010
Crimp Modulus	cr	0.091	0.047
Compression Modulus	co	0.005	0.005
Time constant	t_c	8 μs	2 μs
Density	ρ	2.69e-4 $lb_f s^2/in^3$ 2.88 g/cm^3	2.88e-4 $lb_f s^2/in^3$ 3.08 g/cm^3
Shell thickness	t	0.0031 in./ply (0.008 cm/ply)	0.0020 in./ply (0.005 cm/ply)

2.6 ANALYSIS OF ASU STATIC RING TESTS.

SRI developed a finite element mesh, shown in figure 8, to simulate the static ring tests performed by ASU. The static test apparatus, as shown in figure 8(a), was a 32-in.-diameter, 6-in.-wide steel ring, assumed fixed in space. A 2-in.-wide by 3/8-in.-thick impactor with rounded edges, shown in figure 8(b), was pushed through a machined 3.0-in.-square hole in the ring. For this configuration, the fabric model was a single layer of elements 4 in. wide. The mesh for the fabric, as shown in figure 8(c), was uniform, 1/4-inch-square elements. The mesh for the fragment is also shown in figure 8(c).

2.6.1 Kevlar Ring.

Figure 9 shows the calculated force-displacement relation for the ring test with Kevlar. As the stroke increases, the fabric response stiffens considerably due to both geometric effects and slack in the fabric. For these calculations, the impactor was given a large mass, an initial velocity of 20 m/s, and was constrained to move in the radial direction. In this way, the force on the impactor was calculated by multiplying the deceleration of the impactor by its mass. The simulation time was 80 ms.

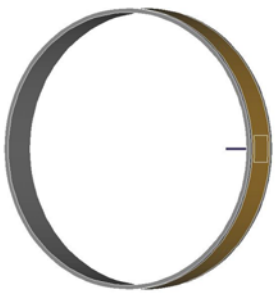

(a) Overall test configuration

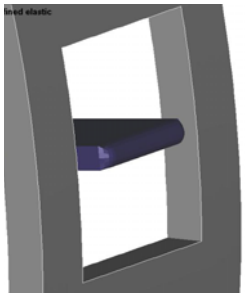

(b) Impactor and hole in steel ring

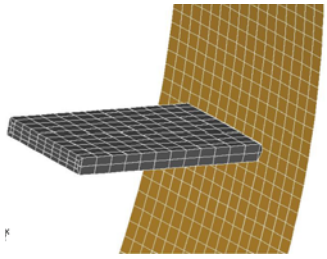

(c) Fabric and impactor mesh

FIGURE 8. FINITE ELEMENT MODEL OF STATIC RING TEST

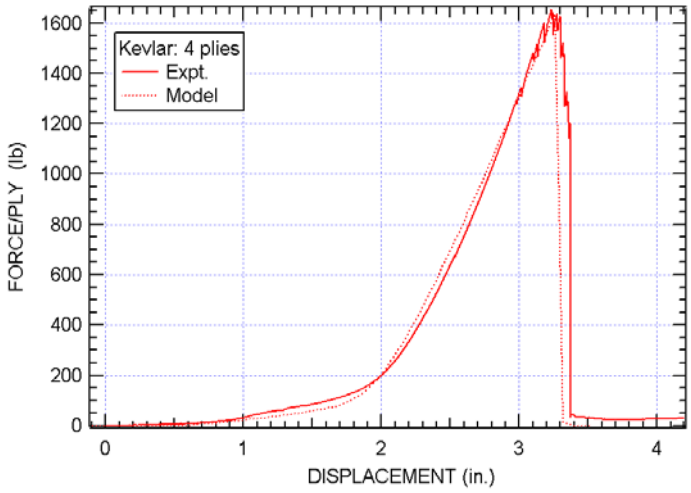

FIGURE 9. CALCULATED FORCE DISPLACEMENT FOR STATIC RING TEST WITH KEVLAR

To account for variations in initial slack and zero settings between the simulation and the experiment, the calculated displacement was shifted (by 0.1 in.) to match the measured displacement at 200 lb. As shown in table 3, the average peak load for the experiments on one, two, four, and eight plies of Kevlar was 1639 lb with a standard deviation of 49 lb. The calculated peak load was 1637 lb. Based on normalized force-displacement curves (all curves set to equal displacements at 200 lb), the average displacement at failure in the experiments was 3.44 in. with a standard deviation of 0.10 in. The calculated value was 3.36 in.

TABLE 3. RING TEST FORCE AND PLY

Plies	Kevlar (lb)	Zylon (lb)
1	1568	1739
2	1680	1704
4	1656	1840
8	1653	1644
Avg.	1639	1729
Std. Dev.	49	82
Model	1637	1493

Figure 10 shows the calculated deformed shape of the fabric along with effective stresses in the fabric at four times intervals, corresponding to impactor displacement values of 1.0, 1.5, 2.0, and 2.1 in. Ripples in the fabric are clearly seen. As shown in figure 10(d), penetration of the fabric initiated near the center of the fabric swath.

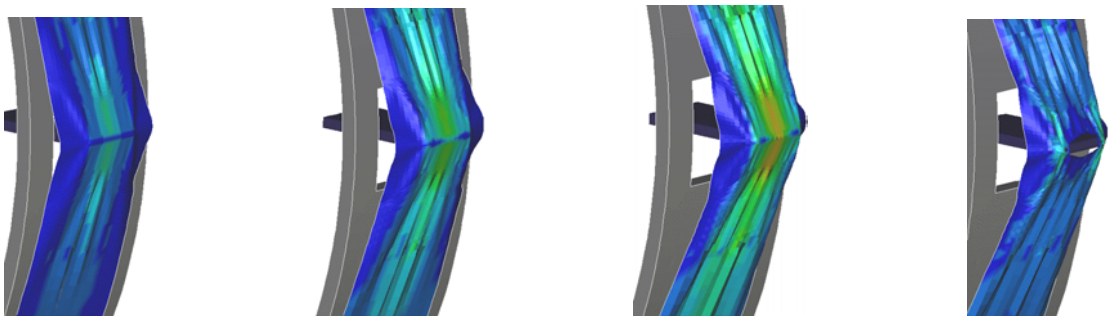

(a) displacement = 1.0 in. (b) displacement = 1.5 in. (c) displacement = 2.0 in. (d) displacement = 2.1 in.

FIGURE 10. CALCULATED RESPONSE OF SINGLE-LAYER ZYLON

This calculation took about 30 minutes when run on four processors of a 16-processor LINUX cluster (eight nodes and two Intel Pentium III-900 MHz processors with 1 GB memory on the master node and 256 MB memory on each slave node).

2.6.2 Zylon Ring.

Figure 11 shows the calculated force-displacement relation for the ring test with Zylon along with the experimental results for eight plies. The response is similar to that for Kevlar, although the displacements are greater because the Zylon fabric has more crimp in the warp direction. To account for variations in the initial slack and zero settings between the experiment and simulation, the calculated displacement was shifted to match the measured displacement at 200 lb. As shown in table 3, the average peak load for the experiments on one, two, four, and eight plies of Zylon was 1729 lb/ply with a standard deviation of 82 lb. The calculated peak load was 1493 lb (about 15% below the average of the tests). The average value of displacement at failure was 4.5 in. with a standard deviation of 0.10 in. The calculated value was 4.4 in. One theory for

this lower prediction is that the failure is so abrupt that the numerical treatment of the contact can lead to early failure prediction.

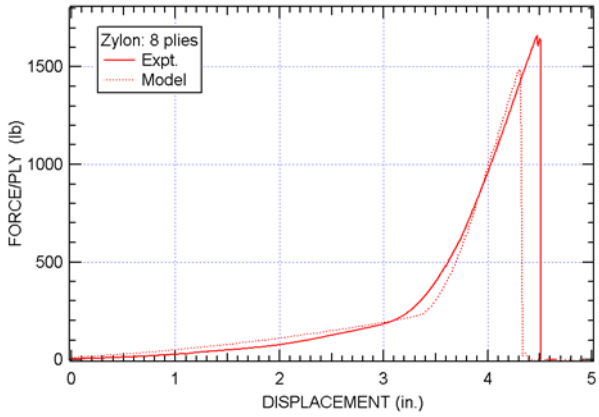

FIGURE 11. CALCULATED FORCE DISPLACEMENT FOR STATIC RING TEST WITH ZYLON

2.7 NASA TESTS.

Two sets of ballistic impact tests were performed at NASA GRC, one set on Zylon and one set on Kevlar. The test setup, shown in figure 12, is similar to the ASU ring tests. A 10-inch-wide fabric swath was wrapped around a 40-inch outside diameter steel ring. The ring was positioned at a 15° angle to allow the impactor to clear the steel ring and impact the center of the fabric swath from inside the steel ring. The steel ring had a 10-inch section missing around the point of impact. More information about the NASA Test Facility is included in reference 3.

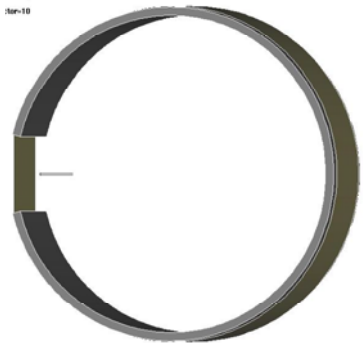

FIGURE 12. TEST SETUP FOR THE NASA BALLISTIC TESTS

The impactor was a 4- by 2- by 5/16-inch-rectangular steel block with rounded edges (5/16-inch radius), as shown in figure 8(b), and a nominal weight of 317 g. The impactor was launched from a gas gun and oriented to hit the fabric, as shown in figure 12, with the narrow side facing a viewer looking at the side of the ring. Because the ring was positioned at a 15° angle relative to the trajectory of the impactor, and the fabric was pulled across the missing section of the ring, one corner of the impactor hit the fabric first.

The velocity of the impactor varied from 345 to 915 ft/s. Tests were performed on Kevlar with 1, 2, 4, 8, 16, and 24 plies of fabric and for Zylon 4, 8, 16, and 24 plies. A list of the test numbers with measured impact velocities and residual velocities are shown in tables 4 and 5.

TABLE 4. BALLISTIC TEST RESULTS FOR KEVLAR

Test No.	No. Plies	Impact Velocity (ft/s)	Residual Velocity (ft/s)
LG434	1	384	361
LG433	1	389	367
Model	1	385	367
LG449	2	345	279
LG444	2	349	278
Model	2	347	310
LG403	4	900	845
LG410	4	912	865
Model	4	900	855
LG424	8	834	744
LG409	8	888	808
LG404	8	897	819
Model	8	900	810
LG432	16	896	650
LG429	16	914	720
Model	16	900	665
LG411	24	886	413
LG405	24	898	496
LG427	24	915	608
Model	24	900	519

TABLE 5. BALLISTIC TEST RESULTS FOR ZYLON

Test No.	No. Plies	Impact Velocity (ft/s)	Residual Velocity (ft/s)
LG412	4	798	733
LG406	4	895	835
Model	4	900	845
LG417	8	892	791
LG413	8	901	776
LG408	8	904	792
LG425	8	908	804
Model	8	900	778
LG426	16	911	630
Model	16	900	614
LG414	24	830	0
LG407	24	904	0
Model	24	900	480

2.7.1 Ballistic Test Simulation Results.

The NASA ballistic tests were simulated with the model. One simulation was performed for each fabric (Kevlar or Zylon) and target thickness (number of plies). As listed in tables 4 and 5, the impact velocity for the simulation was generally chosen as 900 ft/s, except for the cases with one or two plies of fabric. In those cases, a velocity near the average of the test values was chosen. For the simulations, the impactor was assumed to impact the fabric with no yaw or pitch. In the tests, the yaw of the impactor estimated from the videos was typically about 4°.

Figure 13 shows a direct comparison of an experiment and simulation for NASA Test LG408, an eight-ply target of Zylon. The measured impact velocity was 904 ft/s, and the measured residual velocity was 792 ft/s. For the simulation, the impact velocity was 900 ft/s, and the residual velocity was 778 ft/s. Figure 13 shows the deformed fabric at three

different times during the impact. Visually, the deflected shape of the fabric in the simulation is very close to that of the experiment for the three times shown. The fabric is pulled out by the impactor in a diamond-shaped pyramid, and the calculated extent of the deformation matches the experiments well. The impactor starts to become visible through the fabric at 0.35 ms in both the experiment and the simulation. At 0.53 ms, the front of the impactor is clearly visible both in the simulation and the experiment, and it appears that in the model, the fabric has pulled back from the front of the impactor more in the simulation than in the experiment.

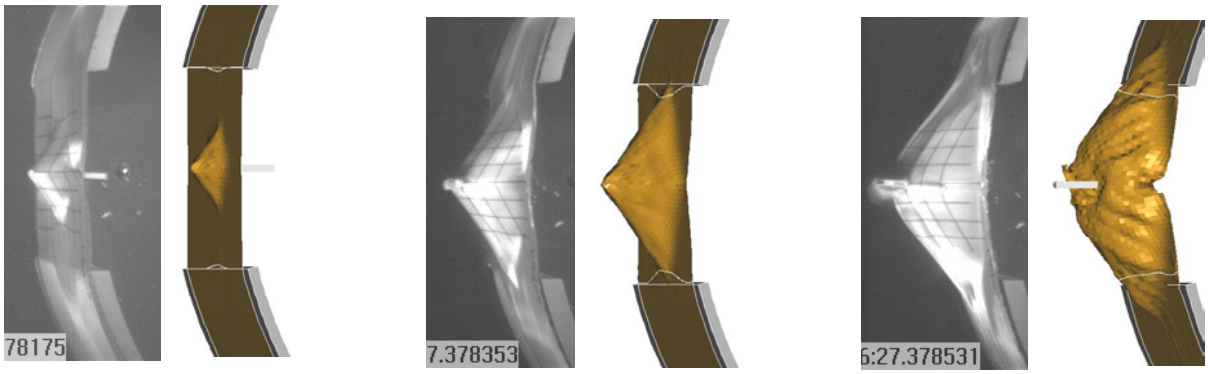

Experiment Simulation time = 0.17 ms | Experiment Simulation 0.35 ms | Experiment Simulation 0.53 ms

FIGURE 13. EXPERIMENT AND SIMULATION RESULTS FOR NASA TEST LG408, EIGHT-PLY TARGET OF ZYLON

2.7.2 Computational Results: Comparing With Data.

To compare the results of the experiments and simulations of the NASA ballistic tests, normalized energy absorbed is plotted as a function of normalized impact energy. The impact energy is the kinetic energy of the impactor (e.g., kJ), and the absorbed energy is the difference between the initial and residual kinetic energy of the impactor. The energies are normalized by the cross-sectional area of the impactor (in this case, 4.03 cm^2), and then, to allow comparisons between different materials and different numbers of plies, the energies are normalized by the areal density of the fabric (e.g., 0.01575 g/cm^2 for Zylon). The figure of merit, i.e., the normalized energy absorbed, is then given in units of (energy/area)/(g/area), corresponding to the energy absorbed for a given weight of fabric.

This choice of normalization quantities is consistent with analyses performed by P. Cunniff of a large collection of ballistic performance data on different types of fabrics [4]. Figure 14 shows V_{50} (velocity at which half the projectiles are stopped) normalized by a material constant $\tilde{U}^{1/3}$ as a function of the areal density of the fabric, A_d, the area of the projectile, A_p, and the mass of the projectile, m_p. Figure 14 shows that a square root function is a good fit to the data, i.e.,

$$\frac{V_{50}}{\tilde{U}^{1/3}} = c\left(100 A_d A_p / m_p\right)^{1/2} \tag{6}$$

where c is a constant. Squaring both sides of the equation and rearranging gives

$$\frac{\frac{1}{2} m_p V_{50}^2}{A_d A_p} = 50 c^2 \tilde{U}^{2/3} \tag{7}$$

Thus, for these test data, the maximum kinetic energy that the target is able to stop normalized by the areal density of the fabric, and the area of the projectile is a constant for each material over the range of velocities and target thicknesses tested.

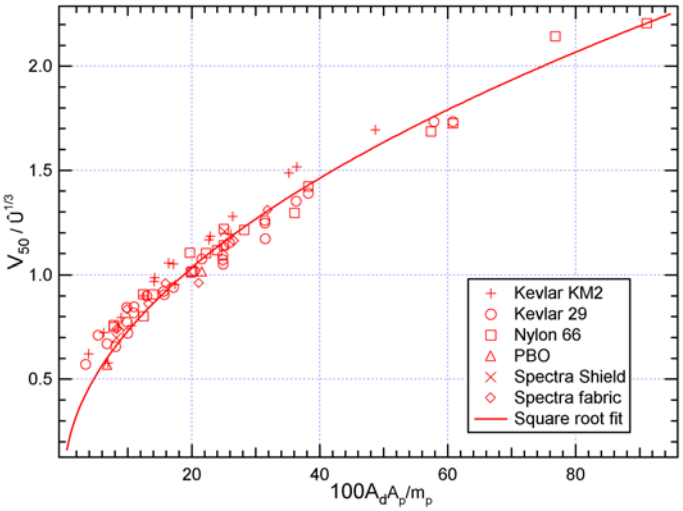

FIGURE 14. DIMENSIONLESS PLOT OF V_{50} RESULTS OF FABRIC ARMOR SYSTEMS
(Illustrating curve fit of experimental data taken from reference 4.)

2.7.3 Kevlar Tests.

Figure 15 shows the results for the NASA tests on Kevlar in terms of normalized energy absorbed as a function of normalized impact energy. In this graph, if each ply of fabric absorbed the same amount of energy, the data would all lie on a horizontal line. The diagonal line corresponds to absorbing 100% of the impact energy (i.e., stopping the impactor). The points to the right of the line absorb less than 100% of the impactor energy. Considering the scatter in the experimental data, the simulations look reasonable for targets with four plies or more. In the one- and two-ply tests, the model absorbs significantly less energy than in the experiments and, also, significantly less energy than in the other simulations. Because the energy absorbed is calculated based on the difference between two large numbers (impact and residual velocity), especially for tests away from the diagonal line of 100% energy absorbed, uncertainties in measuring the velocities can make for a large error in the absorbed energy.

Model results are very sensitive to details of the impact, including stresses developed at the slidelines due to interpenetration of the impactor with the fabric. These slideline forces are typically of high stress and short duration and also appear to be somewhat random. Thus, the variations in the simulations do not always show clear trends. For example, from 8 to 16 plies,

the model absorbs more energy, but for 24 plies, the model absorbs slightly less energy than for 16 plies.

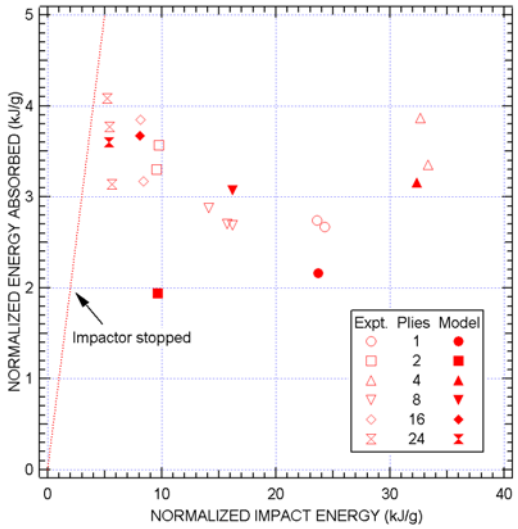

FIGURE 15. SIMULATION RESULTS FOR BALLISTIC TESTS ON KEVLAR FABRIC

2.7.4 Zylon Tests.

Figure 16 shows the results for the NASA tests on Zylon in terms of normalized energy absorbed as a function of normalized impact energy. For these tests, the model does a very good job of matching the data for 4, 8, and 16 plies, but underpredicts the energy absorbed by 24 plies, which stops the impactor in the experiments. In the 4, 8, and 16 plies, the normalized energy absorbed is relatively constant both in the experiments and in the simulations. In comparison to Kevlar, the Zylon absorbed significantly more energy for a given weight of fabric.

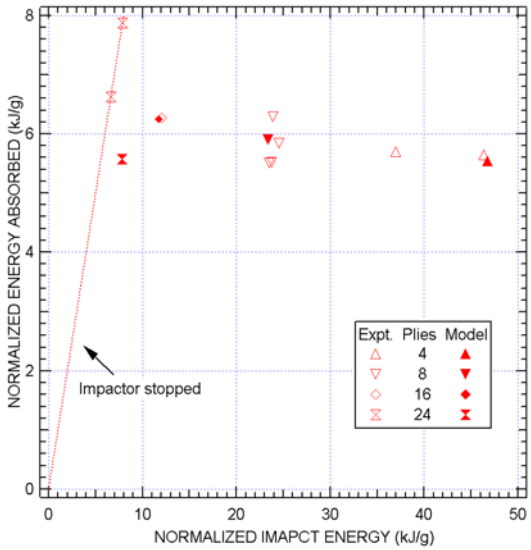

FIGURE 16. SIMULATION RESULTS FOR BALLISTIC TESTS ON ZYLON TARGETS

2.8 DISCUSSION OF RESULTS.

The model predicted absorbed energies that were in general agreement with measurements, although in certain instances, energies were underpredicted in the model. The peak load and strain to failure computed in the quasi-static tests on Kevlar agreed well with measured values; however, the peak load computed for Zylon was about 15% lower than measured. For the ballistic tests, the model predicted the energy absorbed by Kevlar in the 24-layer test, but underpredicted the absorbed energy in the 1-, 2-, and 4-ply tests. For ballistic tests on Zylon, the absorbed energy predicted by the model was within the test data scatter for 4, 8, and 16 layers; however, the model underpredicted the energy absorbed by 24 layers.

The choice of analysis parameters and solution algorithms (particularly the choice of slideline parameters) had a big effect on energy absorbed calculated in the ballistic tests. The sensitivity may be related to the high-amplitude, high-frequency stresses caused by the numerical algorithms used to treat interfaces. The fabric probably exhibited significant damping that minimized these stresses. Future work should investigate material damping.

An improved treatment of rate effects is also needed. Currently, rate effects are included as a simple constant that limits how fast damage can occur. Some data are available for Kevlar that indicate the rate sensitivity of strength and stiffness.

During the project, Honeywell and SRI compared results obtained on different computer platforms and with different versions of LS-DYNA. Significant discrepancies were found, and Livermore Software Technology Company (LSTC) was consulted. LSTC agreed to consider benchmarking LS-DYNA for problems involving containment and uncontainment of engine debris, in the manner they do for automobile crashworthiness problems, to ensure uniform results across platforms and LS-DYNA versions.

A procedure for using multiple layers of shell elements to model many fabric plies will facilitate design computations. Honeywell began to investigate such a procedure for calculating penetration resistance of thick fabric layers, which is addressed in reference 1. Such an effort needs to involve both material model development and treatment of slidelines.

Additional information is available that would be useful in checking and further developing the model. In particular, the high-speed videos of the deforming fabric provided velocity history data that could be compared with computed histories to determine if the forces on the impacting and decelerating fragment are correct.

Finally, for robustness and to ensure applicability to engine burst scenarios, additional experimental data should be acquired. Ballistic experiments should be performed in which sharper projectiles more representative of fan blade fragments impinge at oblique angles on multiple-layer fabric targets.

2.9 OTHER ITEMS WORTHY OF CONSIDERATION AND FURTHER INVESTIGATION.

- Sensitivity of model to slideline parameters. The cause of slideline parameter sensitivity should be investigated. The sensitivity may be related to the nonphysical high-amplitude,

high-frequency forces at yarn intersections predicted by the numerical algorithms. In reality, however, the fabric probably damps these forces.

- Sensitivity of model to material parameters. Simulations of quasi-static and ballistic ring tests should be performed in which material constants, mesh size, and fragment orientation (pitch and yaw) are varied to determine model sensitivity to these parameters.

- LS-DYNA benchmarks for containment and uncontainment problems. LSTC should establish several well-defined scenarios as standards to allow designers to benchmark their computations and ensure that the LS-DYNA code gives consistent results across platforms and across versions.

- Rate effects on fabric deformation and failure. The treatment of rate effects should be improved. Rate effects are currently accounted for by a simple time constant that limits how fast damage can occur. Guidance can be obtained from data that exist on the strength and stiffness of Kevlar fabrics.

- Use of several layers of elements to model multiple-fabric plies. The effort begun by Honeywell to investigate using multiple layers of shells to model thick fabric layers should be continued because multilayer shells indicate better how many layers of fabric would be penetrated for a given threat. The effort should involve both material model development and slideline treatment.

- Fabric deformation profiles. Frames from the high-speed videos of the ballistic tests should be analyzed to extract data for checking and refining the model. The deformation profiles of the impacted fabric as a function of time should be compared with velocity histories of the impactor to determine if the fabric model is correctly applying forces as the fabric deforms.

- More representative engine burst experiments. Ballistic experiments should be performed in which sharper projectiles more representative of fan blade fragments impinge at oblique angles on multiple-layer fabric rings. The data and observations will help ensure applicability to engine burst scenarios.

3. SWATH PUSH TESTS.

SRI performed a series of quasi-static push tests on 1.5-in.-wide swaths of the baseline Kevlar and Zylon fabrics to (1) help determine material properties for modeling the impact response of multiple plies of fabric, and (2) investigate the unloading and reloading response of these fabrics.

The setup and analysis procedures for the swath push tests are described in appendix B. A 1.5-in.-wide, 7.2-inch-long fabric swath is gripped at two ends and is quasi-statically loaded in the center by a round-edged, 2-inch-wide penetrator. The load on the penetrator and deflection of the fabric are measured, and the stress and strain in the fabric is calculated using geometric relationships.

A matrix of the parameters and results of the multiple-ply tests (tests 22-31) and cyclic unloading tests (tests 33-35) is shown in table 6, along with those of the previously reported single-ply, 1.5-in.-wide swath push test (tests 6-10).

TABLE 6. SUMMARY OF SWATH TEST DATA ON 1.5-in.-WIDE BASELINE FABRIC SWATHS

Test No.[a]	Target[b]		No. Plies	Areal Density	Fabric Width		Max. Load		Energy Absorbed[c]				SEA[d]		Comments
	Material	Weave (Yarn/in.)		(g/cm^2)	(in.)	(Yarns)	(lb)	per Ply (lb)	(J)	(ft-lb)	(J)	per Ply (ft-lb)	$\frac{J}{g/cm^2}$	$\frac{ft\text{-}lb}{lb/ft^2}$	
6	Kevlar	17x17	1	0.02275	1.47	25	530	530	26	19	26	19	1157	417	Single-Ply Tests
8	Kevlar	17x17	1	0.02275	1.47	25	570	570	25	19	25	19	1113	401	
7	Zylon	35x35	1	0.01575	1.43	50	760	760	40	29	40	29	2517	906	
10	Zylon	35x35	1	0.01575	1.43	50	839	839	30	22	30	22	1891	681	
24	Kevlar	17x17	2	0.0455	1.47	50	1093	547	45	33	22	16	980	353	Multiple-Ply Tests
25	Kevlar	17x17	2	0.0455	1.47	50	1049	525	55	41	28	20	1219	439	
31	Kevlar	17x17	4	0.091	1.47	100	1635	409	85	63	21	16	936	337	
27[e]	Kevlar	17x17	8	0.182	1.47	200	>2256	>282	>244	>180	>31	>23	>1343	>484	
28[e]	Kevlar	17x17	8	0.182	1.47	196	>2256	>282	>234	>173	>29	>22	>1286	>463	
30	Kevlar	17x17	8	0.182	1.47	197	2462	308	225	166	28	21	1238	446	
22	Zylon	35x35	2	0.0315	1.43	100	1229	615	>148	>109	74	54	>4684	>1686	
23	Zylon	35x35	2	0.0315	1.43	100	1287	644	>119	>88	>59	>44	>3768	>1357	
32	Zylon	35x35	4	0.063	1.43	200	1922	481	----	----	----	----	----	----	Major Slip at Grips
35	Kevlar	17x17	1	0.02275	1.47	25	580	580	----	----	----	----	----	----	Cyclic Unload
33	Zylon	35x35	1	0.01575	1.43	50	735	735	----	----	----	----	----	----	Cyclic Unload
34	Zylon	35x35	1	0.01575	1.43	50	744	744	----	----	----	----	----	----	Cyclic Hold

a. All tests involve the baseline fabrics used in this program. All tests used the 2-in.-wide rounded-end penetrator (same as that used by ASU), a stroke rate of 0.05 in./s. and the yarns tested were all in the warp direction.

b. Distance between grips was approximately 7.2 in.

c. Equals the area under the load-deflection curve.

d. SEA = Specific Energy Absorbed = energy absorbed divided by areal density of the target

e. Load record cut off above 2256 lb for these two tests.

3.1 SWATH PUSH TEST RESULTS.

Tests were performed to investigate the response of two, four, and eight plies of Kevlar, and these results, along with those from the previously performed single-ply Kevlar tests, are shown in figures 17 and 18. To normalize the results for all the tests, figure 17 shows the load per ply as a function of stroke, and figure 18 shows the stress-strain results.

For the case of Zylon, four- and eight-ply tests could not be performed due to significant slip at the grips, so only two-ply tests were reported (and even those had a slight amount of slip at the grips). Figures 19 and 20 show the two-ply Zylon results, compared with the previously reported single-ply results.

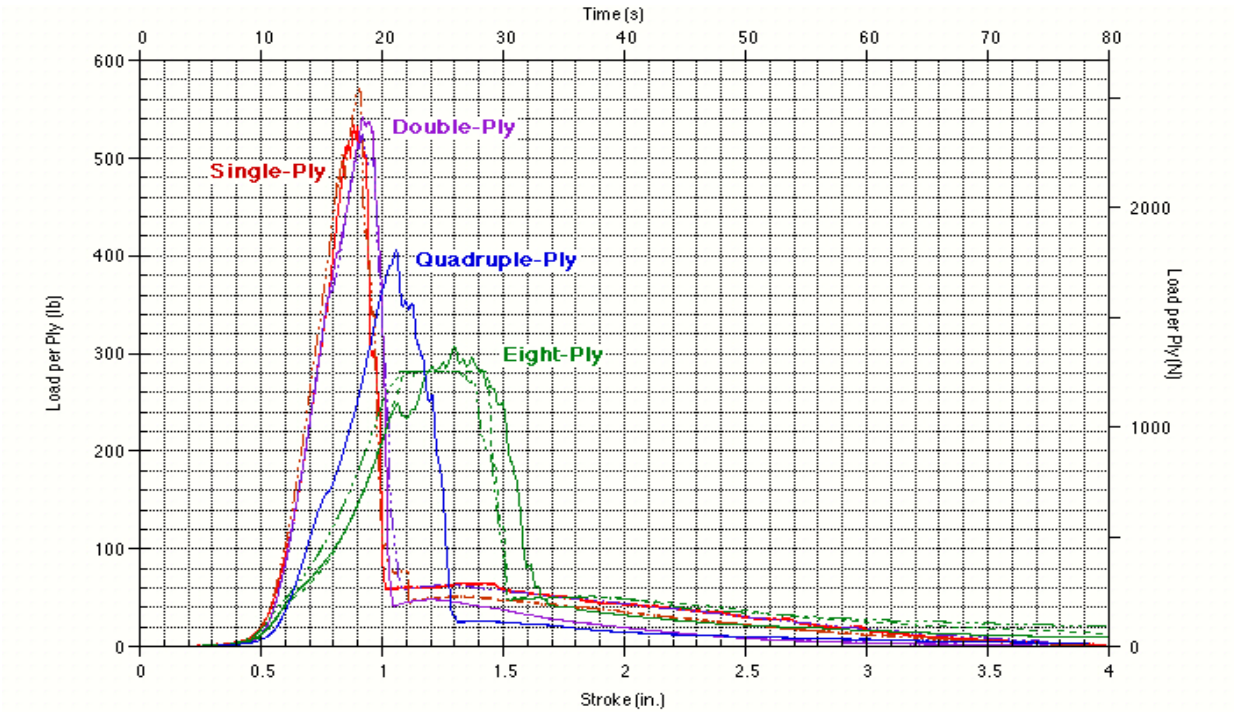

FIGURE 17. LOAD-STROKE RESPONSE OF KEVLAR SWATHS

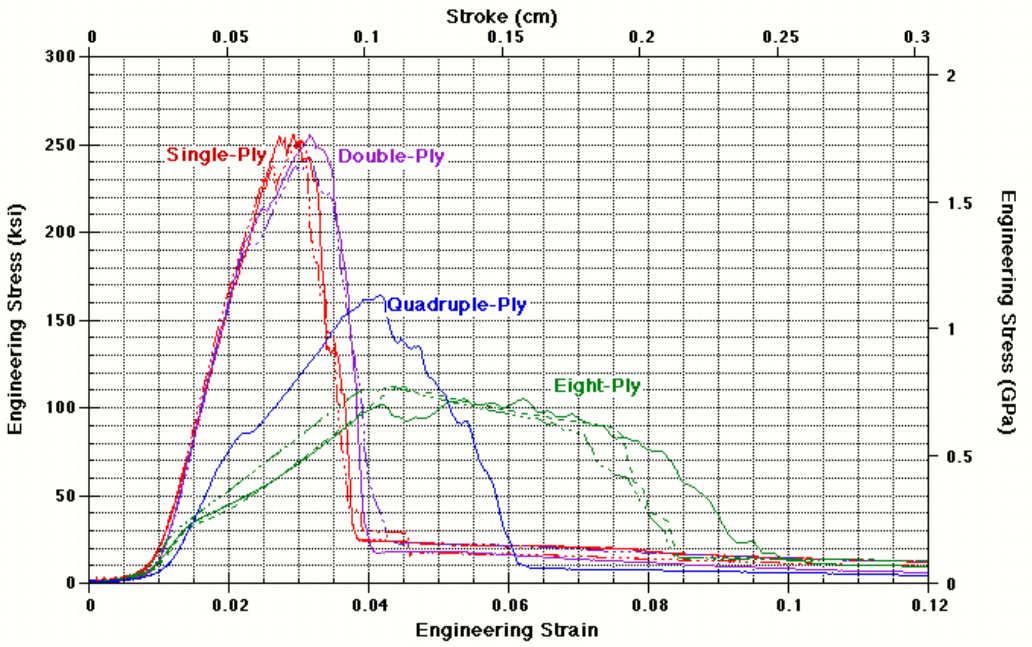

FIGURE 18. STRESS-STRAIN RESPONSE OF KEVLAR SWATHS

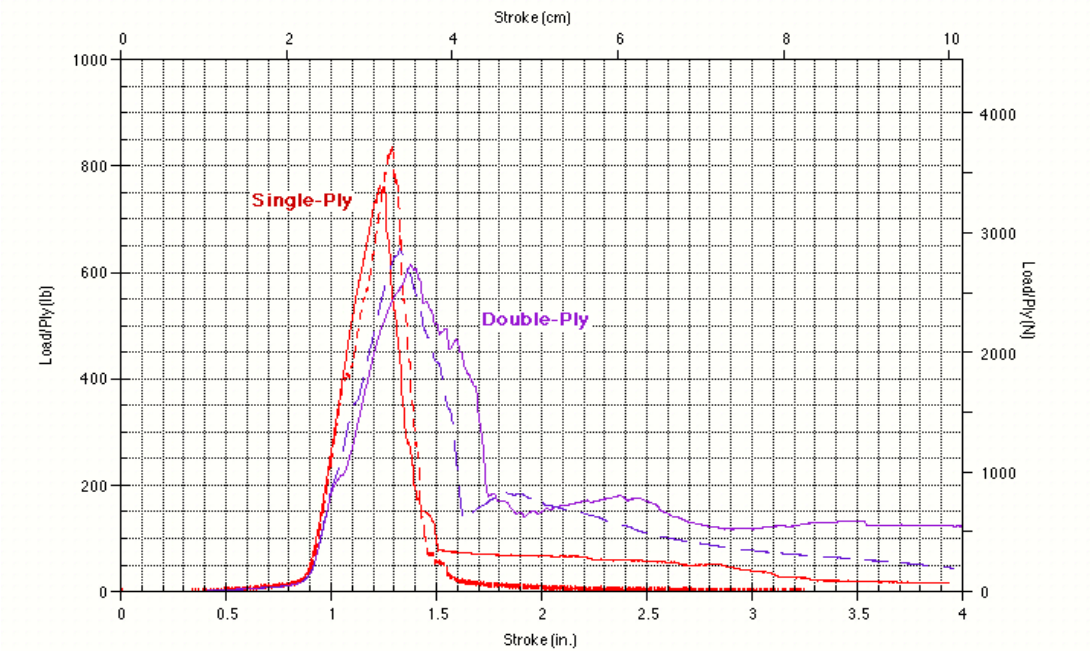

FIGURE 19. LOAD-STROKE RESPONSE OF ZYLON SWATHS

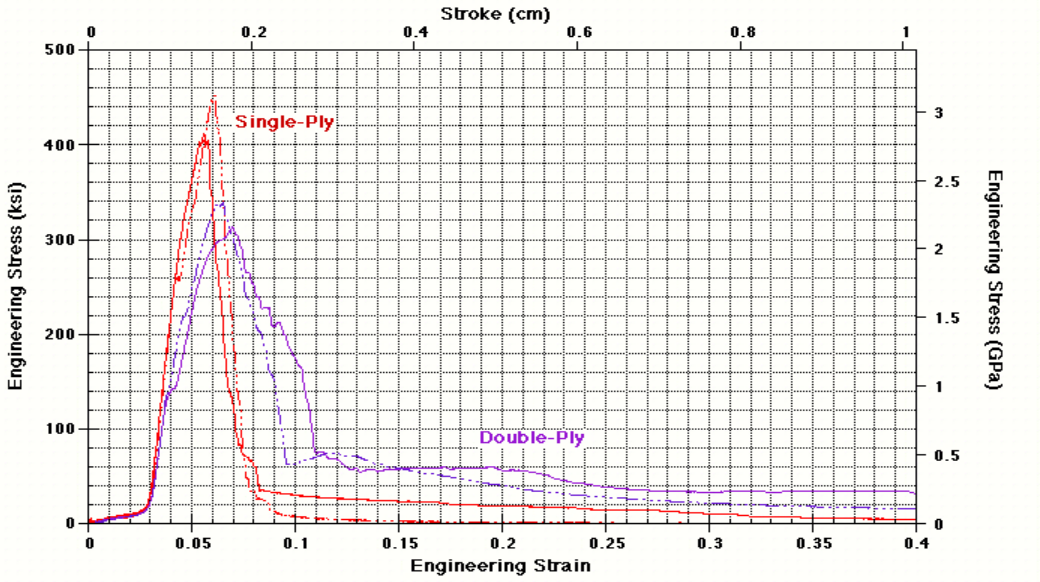

FIGURE 20. STRESS-STRAIN RESPONSE OF ZYLON SWATHS

3.2 MULTIPLE-PLY SWATH PUSH TEST RESULTS.

For both fabrics, the overall trend was that, as the number of plies increases, the loading modulus and the peak load (or peak stress) decrease, while the strain at peak and strain at failure increase (greater spread). The area under the curve in all cases remains relatively constant. Repeat tests showed some scatter, but the trend was significant and consistent.

This trend was consistent with combining curves that have the same shape, but were offset from each other. An example is shown in figure 21. Two curves for one-ply Kevlar offset by 1% strain are averaged. The resulting curve has the response characteristics seen in the tests: lower initial modulus, lower peak, and greater spread.

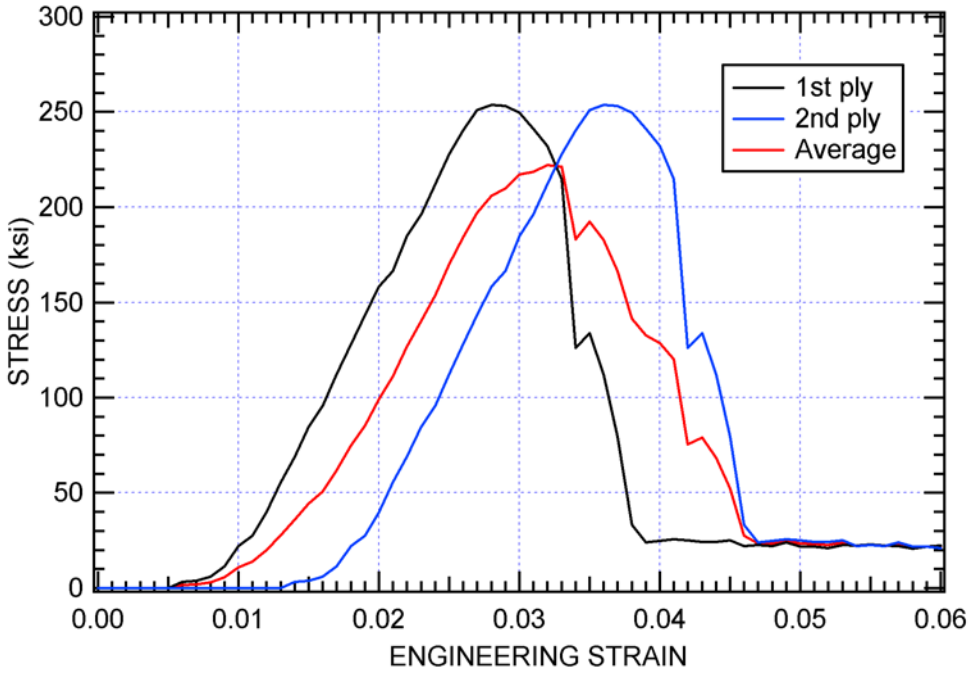

FIGURE 21. AVERAGING TWO KEVLAR PLIES DISPLACED BY A STRAIN OF 0.01

The response of multiple plies can be offset from each other for several reasons. First, in any multiple-ply impact configuration, inner plies are impacted before outer plies. Second, any differences in slack among the plies will have the effect of offsetting the curves with respect to each other. For the swath push test configuration, the two ends of the specimen are wrapped around a flattened bar and then clamped between two plates. As the clamping is increased, the outermost wrapped plies will be stretched more than the inner plies. This effect is, of course, very dependent upon the test configuration. Presumably, if all the plies are prepared with a known prestress, as in the NASA GRC tests, any effect due to different amounts of slack would be minimized.

A model was developed for the response of multiple plies by combining the single-ply response for several plies offset by a specified amount of strain. Figure 22 shows the predicted response of two, four, and eight plies of Kevlar, using the single-ply response with an assumed strain offset of 0.077 between plies. The effect of reducing the peak and spreading the curve is slightly overpredicted for two plies, but shows reasonably good agreement for four and eight plies.

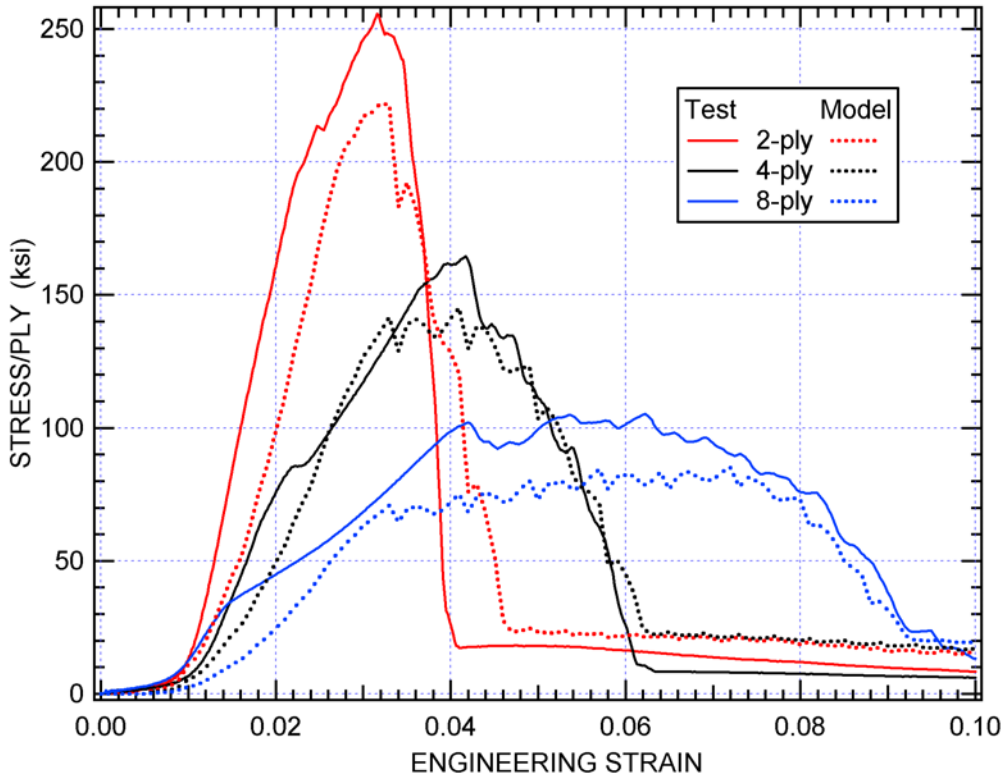

FIGURE 22. STRAIN OFFSET MODEL RESULTS FOR TWO-, FOUR-, AND EIGHT-PLY KEVLAR

3.3 UNLOADING BEHAVIOR.

Cyclic-loading swath push tests were performed on single plies of Kevlar and Zylon to determine the unloading and reloading response. For each test, the fabric was partially unloaded and then reloaded several times throughout the test. The response of Kevlar is shown in figure 23, and the response of Zylon is shown in figure 24. The fabrics show similar response. In all cases, the loading and reloading response is nearly elastic, i.e., the curves show little hysteresis. However, unloading does not follow the original loading curve. When the fabric is unloaded before the peak load is reached, the unloading modulus is stiffer than the loading response. The unloading modulus progressively decreases for unloading after the peak. As shown in figure 24, a cyclic test with very slight unloading (over the same time as the full unloading in the other tests) was performed to determine how much of the unloading response was due to relaxation of the fabric at constant strain. The effects of relaxation were not significant.

A possible explanation for the observed response is that during loading, the yarns rearrange and on unloading do not re-rearrange to the initial configuration. After peak load, fibers are broken, therefore, the unloading modulus decreases.

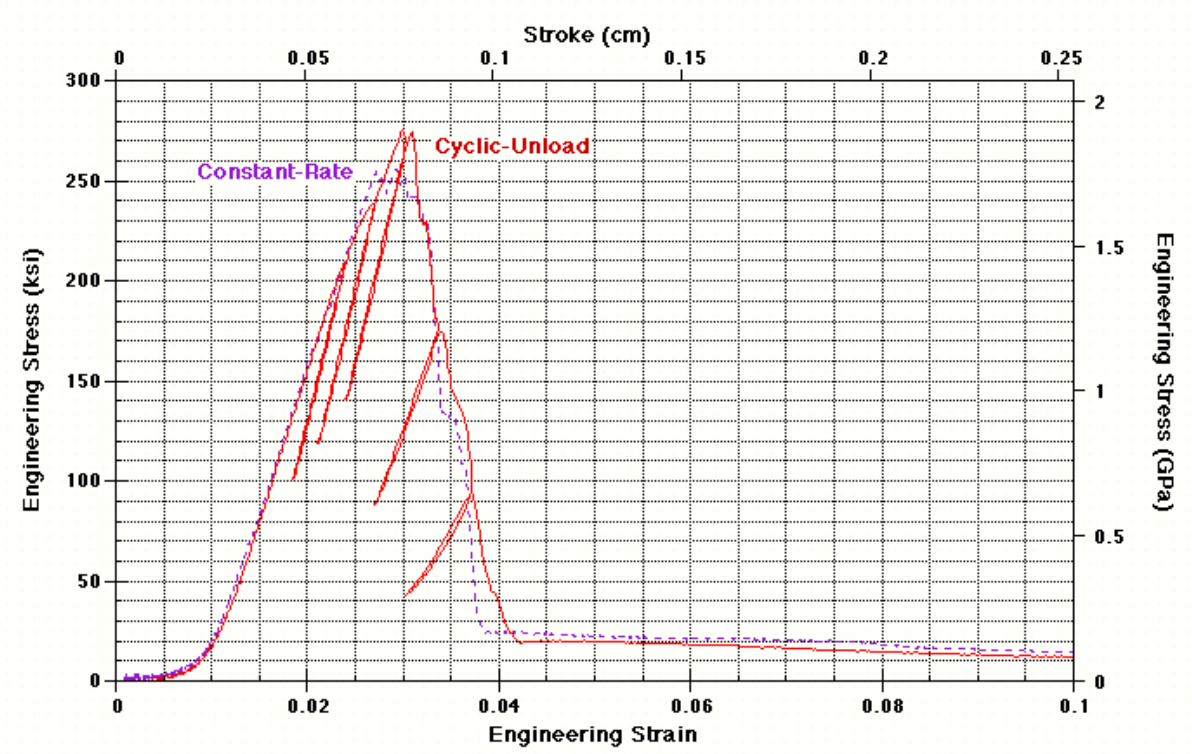

FIGURE 23. CYCLIC UNLOADING RESPONSE OF KEVLAR SWATHS

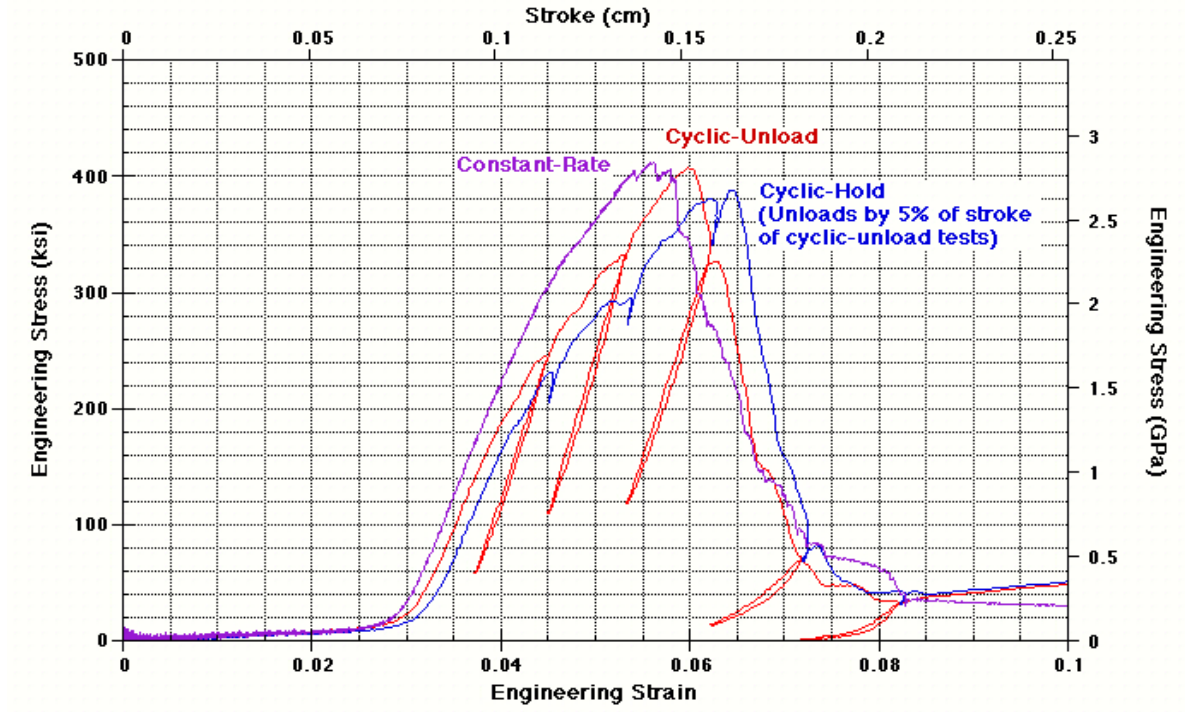

FIGURE 24. CYCLIC UNLOADING RESPONSE OF ZYLON SWATHS

3.4 SUMMARY.

SRI successfully performed several quasi-static push tests on Zylon and Kevlar fabrics, which provided the material properties and the unloading are reloading properties. This data was used in the analyses performed by SRI, ASU, and Honeywell, which is documented in this comprehensive FAA report.

4. REFERENCES.

1. Gomuc, Reha, "Explicit Finite Element Modeling of Multilayer Composite Fabric for Gas Turbine Engines Containment System, Part 4: Model Simulations for Ballistic Tests, Engine Fan-Out, and Generic Engine," FAA report DOT/FAA/AR-04/40,P4, 2004.

2. Rajan S.D., Mobasher B., Sharda J., Yanna V., Deenadayla C., Lau D., and Dhah D., "Explicit Finite Element Modeling of Multilayer Composite Fabric for Gas Turbine Engines Containment System, Part 1: Static Tests and Modeling, FAA report DOT/FAA/AR-04/40,P1, 2004.

3. Periera, M. and Revilock, D., "Explicit Finite Element Modeling of Multilayer Composite Fabric for Gas Turbine Engine Containment Systems, Part 2: Ballistic Impact Testing," FAA report DOT/FAA/AR-04/40,P2, 2004.

4. Cunniff, P.M., "Dimensionless Parameters for Optimizations of Textile-Based Body Armor Systems," *Proceedings of the 18th International Symposium on Ballistics*, San Antonio, TX, November 1999.

APPENDIX A—USER'S GUIDE

USER-DEFINED MATERIAL TYPE 47 (BALLISTIC FABRIC)

LS-DYNA reserves material types 41-50 as user-defined materials. Material type 47 was arbitrarily chosen for implementation of ballistic fabric.

Columns		Quantity	Format
Card 3			
1-10	E	Tensile modulus	E10.0
11-20	ε_{min}	Bidirectional failure strainStrain at first nonlinearity	E10.0
21-30	ε_{max}	Strain at peak stress	E10.0
31-40	σ_{max}	Peak stress	E10.0
41-50	ε_{crx}	Crimp strain, local x direction	E10.0
51-60	ε_{cry}	Crimp strain, local y direction	E10.0
61-70	ε_{soft}	Softening strain, (default = 0.01)	E10.0
71-80	cr	Crimp stiffness, as fraction of E (default = 0.01)	E10.0
Card 4			
1-10	co	Compression stiffness, as fraction of E (default: 0.02)	E10.0
11-20	2G	Shear modulus, (default: 0.02*E)	E10.0
21-30	ε_{tcr}	Transition strain for uncrimping (default = 0.005)	E10.0
31-40	ε_{tul}	Transition strain for unloading (default = 0.005)	E10.0
41-50	ε_{fail}	Strain at failure (default = 5.0*ε_{max})	E10.0
51-60	dd_{max}	Maximum increment in damage per step (default, 0.01)	E10.0
61-70	t_c	Time constant for damage rate (default = 1.0e-6)	E10.0

The ballistic fabric model is orthotropic with stress-strain response as shown in figure A-1 for each of the two yarn (local x and y) directions. The stress-strain responses in the two directions are uncoupled, but the failure response is coupled.

$$\sigma_{xx} = f(\varepsilon_{xx})$$

$$\sigma_{yy} = f(\varepsilon_{yy})$$

$$\sigma_{zz} = 0$$

$$\tau_{xy} = G\,\varepsilon_{xy}$$

$$\tau_{yz} = G\,\varepsilon_{yz}$$

$$\tau_{zx} = G\,\varepsilon_{zx}$$

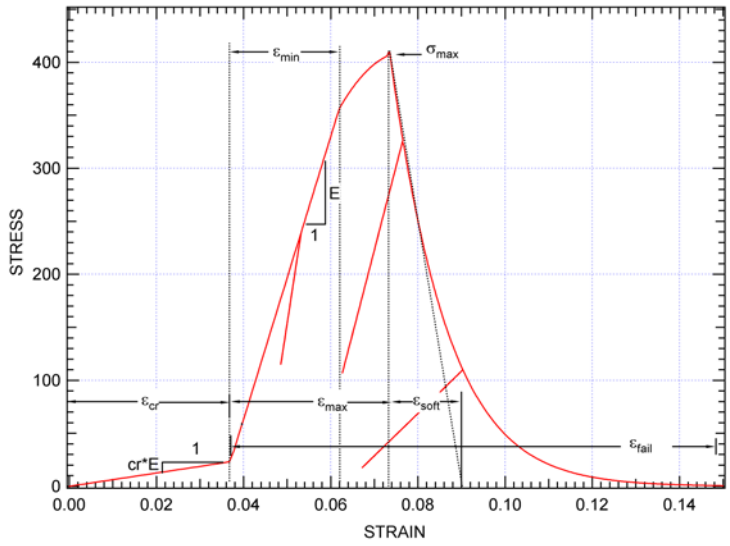

FIGURE A-1. UNIAXIAL STRESS-STRAIN CURVE FOR BALLISTIC FABRIC MODEL

As shown in figure A-1, the uniaxial response has the following features:

- Initial crimp before straightening, prestraighted modulus = cr*E
- Linear response after straightening with modulus E up to a strain of first nonlinearity, ε_{min}
- Peak stress, σ_{max}, and strain at peak stress, ε_{max}
- Linear elastic unloading with modulus of 2E and with reduced modulus with damage
- Postpeak softening
- Failure (element erosion) at full damage

A.1 FITTING MODEL PARAMETERS FROM STRESS-STRAIN CURVES.

A procedure for fitting constants to an existing stress-strain curve is described below and demonstrated for Kevlar 49® in figure A-2, as tested at SRI International. Note that the values listed in table A-1 are taken from a collection of curves; therefore, they are different from those given is this example.

1. Identify the peak stress σ_{max}.

2. Draw a line tangent to the loading curve at half the peak stress to get the loading modulus, E.

3. Fit a line to the initial portion of the loading curve to get the crimp stiffness factor, cr.

4. For the descending portion of the curve, draw a tangent at 0.8 σ_{max}.

5. Identify the amount of crimp strain, ε_{cr}, where the crimp stiffness line crosses the loading line.

6. Starting from ε_{cr}, identify ε_{min}, the strain at which the curve departs from linearity, and the strain at peak stress, ε_{max}.

7. Starting from ε_{max}, identify ε_{soft}, where the unloading tangent crosses the x-axis.

8. Calculate the shell element thickness as one-half the areal density of the fabric divided by the material density. For density, ρ, use twice the solid density of the material.*

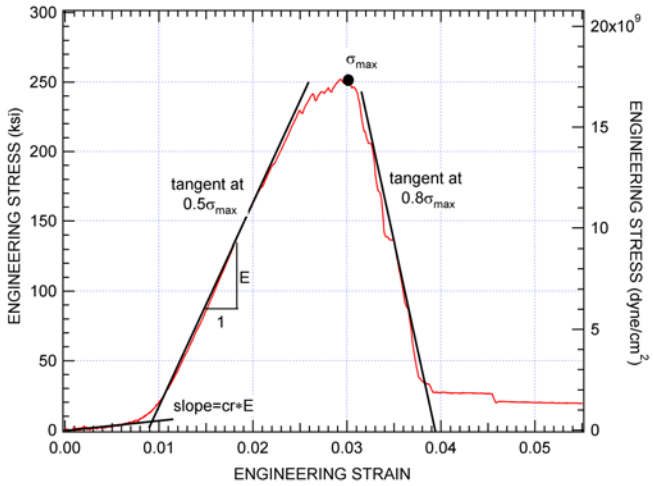

(a) steps 1-4

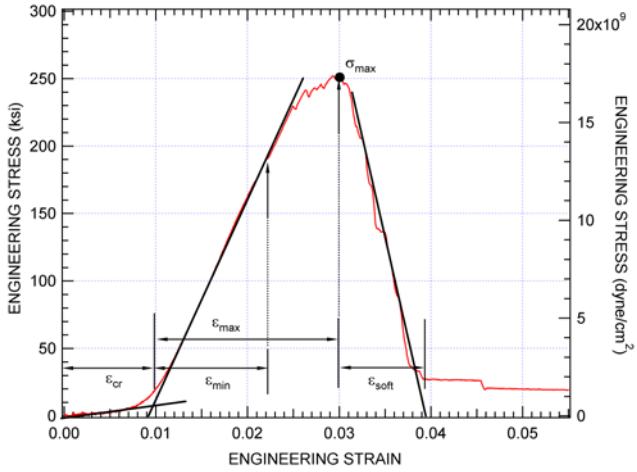

(b) steps 5-7

FIGURE A-2. DEMONSTRATION OF FITTING CONSTANTS TO A STRESS-STRAIN CURVE FOR KEVLAR

* The effective thickness for the fabric is given by the areal density of the fabric divided by the material density. However, for woven fabric, only half the yarns provide stiffness in a given direction. Therefore, in order to use the measured modulus, only half the effective thickness of the fabric should be used for the shell thickness. To keep the correct mass properties, the density must be twice the solid density of the material.

TABLE A-1. CONSTANTS FOR KEVLAR AND ZYLON

Name	Symbol	Kevlar 49	Zylon
Tensile Modulus	E	10.2 Msi (70.3 GPa)	13.3 Msi (91.7 GPa)
Peak stress	σ_{max}	0.305 Msi (2.10 GPa)	0.421 Msi (2.90 GPa)
Initial damage strain	ε_{min}	0.0235	0.025
Strain at peak stress	ε_{max}	0.0262	0.036
Crimp strain x direction	ε_{crx}	0.01	0.037
Crimp strain y direction	ε_{cry}	0.01	0.006
Failure strain	ε_{fail}	0.010	0.010
Crimp Modulus	cr	0.091	0.047
Compression Modulus	co	0.005	0.005
Time constant	t_c	8 μs	2 μs
Density	ρ	2.69e-4 $lb_f s^2/in^3$ 2.88 g/cm^3	2.88e-4 $lb_f s^2/in^3$ 3.08 g/cm^3
Shell thickness	t	0.0031 in/ply (0.008 cm/ply)	0.0020 in/ply (0.005 cm/ply)

A.2 PROCEDURE FOR AVERAGING RESULTS FROM MULTIPLE STRESS-STRAIN CURVES.

For multiple stress-strain curves, use the following procedure to average the curves.

- For each curve, identify a peak stress, σ_{max}.
- Calculate an average peak stress, $\overline{\sigma}_{max}$.
- For each curve, identify the strain value at half the average peak stress, ε_{50}.
- Calculate an average value for the strain at half the peak stress, $\overline{\varepsilon}_{50}$.
- Shift curves so that strain equals $\overline{\varepsilon}_{50}$ at $0.5\,\overline{\sigma}_{max}$.
- Calculate an average stress-strain curve from the shifted curves by averaging the stresses at each strain value.

APPENDIX B—SRI SUMMARY REPORT, MARCH 2002

Summary Report • March 2002

Explicit Finite Element Analysis Modeling of Multi-Layer Composite Fabric for Gas Turbine Engines Containment Systems

Donald A. Shockey, Associate Director
Jeffrey W. Simons, Senior Engineer
David C. Erlich, Physicist III
Center for Fracture Physics

SRI Project P11546
Covering the Period from Sept 2001 through March 2002

Prepared for:

Department of Civil and Environmental Engineering
Arizona State University
Tempe, Arizona 85287-5306

ATTN: Dr. S. D. Rajan
Ms. Deborah Shaver

Approved:

Angel Sanjuro, Director
Materials Research Laboratory

FIGURES

TABLES

INTRODUCTION

As part of FAA's AACE program entitled "Explicit Finite Element Analysis Modeling of Multi-Layer Composite Fabric for Gas Turbine Engines Containment Systems," SRI International is providing experimental and computational support to the team led by Arizona State University (ASU) and including Honeywell Engines & Systems Phoenix and NASA Glenn Research Center (GRC). The overall goals of the program are to investigate the use of Kevlar and Zylon in containment barriers against aircraft engine debris and to develop finite element capabilities for barrier design and analysis.

The program is organized in two phases. Phase I includes experiments and analyses of static tests performed at ASU investigating the response of a penetrator pushed through wrapped plies of Kevlar and Zylon. Phase 2 includes experiments and analyses of ballistic tests of the same configuration to be performed at NASA. This report summarizes SRI's contributions to Phase 1.

ANALYSIS

Finite element analysis of ASU static test with Zylon

SRI developed a finite element mesh, shown in Figure 1, for the static tests planned by ASU. The static test apparatus, as shown in Figure 1a, was a steel ring 32 in. in diameter and 6 in. wide. A 2-in.-wide by 3/8-in.-thick-penetrator with rounded edges, shown in Figure 1b, was pushed through a machined 3.0-in.-square hole in the ring. For this configuration, the fabric was a single 4-in.-wide ply of Zylon AS 35x35.

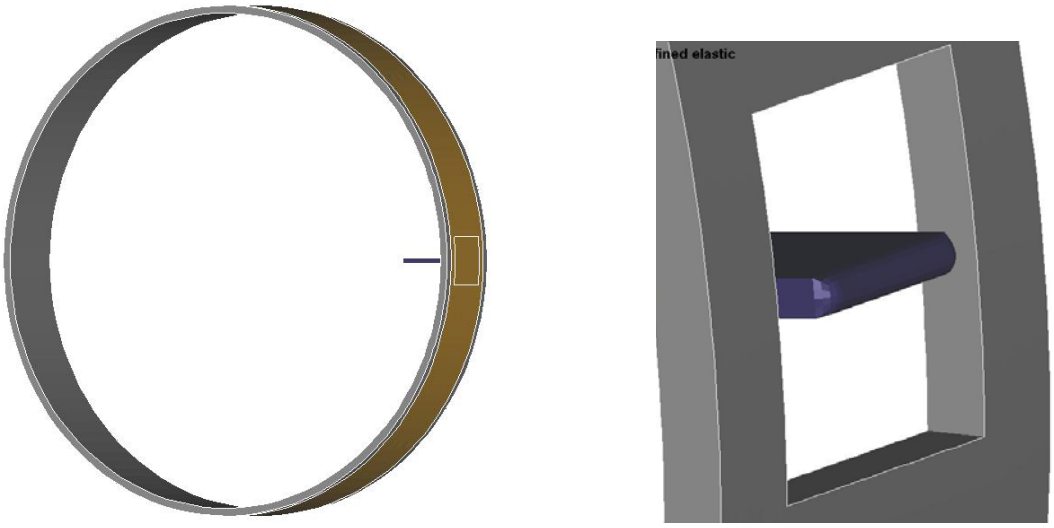

a) Overall test configuration b) Penetrator and hole in steel ring

Figure 1. Finite element model of ASU static test

The finite element analysis was performed using LSDYNA. The finite element model contained 4688 solid elements for the penetrator and the steel ring and 4192 thin shell elements for the fabric. Figure 2 show the calculated force-displacement relation for the

penetrator. As the stroke increases, the fabric response stiffens considerably due to geometric effects. The steps in the curve occur because the analysis was run dynamically; the penetrator impacts the fabric at 20 m/s, and the simulation time is 3.0 ms. The dynamic component of the response could be reduced by lowering the impact velocity, but at the cost of increased CPU time. This calculation took about 20 minutes when run on a single processor of our 16-processor LINUX cluster.

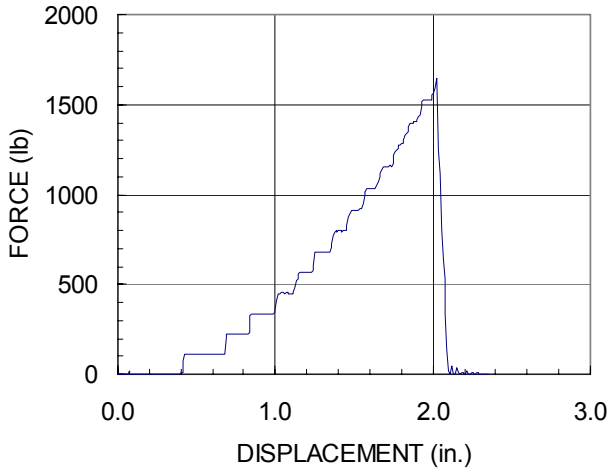

Figure 2. Calculated force displacement for ASU static test with Zylon.

For these simulations we did not include slack in the fabric, which depends on how the test article is fabricated (e.g., how much the fabric is pretensioned). The amount of slack will change both the load and displacement response of the fabric on the penetrator. Without considering slack we estimated a peak load of about 1600 lb. for a single ply of Zylon at a displacement of about 2 in.

Support for Advancing Honeywell's Analytic Capabilities

To assist Honeywell enhance analytic capabilities, SRI provided Honeywell with the source code for SRI Zylon fabric model and step-by-step instructions on how to implement user-defined materials into LSDYNA. As part of this effort, SRI provided several LSDYNA input files for simulating the ASU static tests, including files with the fabric modeled as a: (1) standard elastic material, (2) user-defined elastic material model 41 and (3) SRI's Zylon fabric model as a user-defined material number 47. With each input file SRI also provided Honeywell with Microsoft Excel spreadsheet files containing the calculated force-displacement results of the calculations and estimates of computational times for completion. SRI provided Honeywell with an input file for SRI's Zylon material model written in keyword format so that Honeywell could more easily modify the input. In addition, SRI also provided Honeywell with LSDYNA input files for simulations of SRI push tests P25 and P47.

In order to implement the user-defined materials, SRI modified Honeywell's version of the LSDYNA subroutine dyn21.F and included in that file the FORTRAN source code for SRI's Zylon fabric model. To aid Honeywell's understanding of the source code and to help simplify its use, SRI inserted explanatory comment cards for many of the source

code lines and added default values for many of the required material parameters for the Zylon fabric model.

SRI also provided Honeywell with a user's guide for the Zylon material model. The User's guide was written in a style consistent with the LSDYNA Structured User's manual. It is included in this document as Appendix 1.

EXPERIMENTS: Push Tests on Fabric Swaths

Test Configuration

SRI performed a series of push tests on the Zylon AS 35x35 and Kevlar 29 17x17 fabric. The properties are listed in Table 1.

The test set-up is shown in Figure 3. The test specimen was a 12-in.-long swath of fabric, either 4 or 1.5 in. wide, gripped at 7.25 in. and loaded quasistatically by a steel penetrator at the center of the fabric swath. The penetrator, shown in Figure 4, is a 2.0-in.-wide 5/16-in.-thick steel penetrator had rounded ends with a 5/32 in. radius of curvature in two directions. During the test force and displacement on the penetrator were measured and the response of the fabric in two directions was recorded on videotape.

For the 1.5-in. swaths, the width of the fabric was less than the 2.0 in. width of the penetrator. Based on our previous experience with push tests of single yarns by rounded-end penetrators, these fabric swath push tests should yield stress-strain curves that are similar to uniaxial strain tensile test results.

Table 1. Properties of Zylon and Kevlar Fabrics tested by SRI

WOVEN FABRICS USED IN ASU / HONEYWELL / SRI / FAA PROGRAM			
Trade Name		Zylon-AS	Kevlar-29
Material		Poly-benzobisoxazole (PBO)	P-Aramid
Volume Density (from manufacturer)	(g/cm^3)	1.54	1.44
Yarn Denier - Nominal	(g/9 km)	500	1420
Yarn Denier - Measured	(g/9 km)	500	1490
Measured Linear Density	(mg/cm)	0.556	1.656
Yarn Cross-sectional Area	(cm x 10^{-4})	3.61	11.50
	(in. x 10^{-5})	5.59	17.82
Mesh Density	(yarns/in.)	35x35	17x17
Fabric Thickness (approx.)	(in.)	0.008	0.011
	(mm)	0.21	0.28
Fabric Areal Density - measured	(g/cm^2)	0.01575	0.02275
	(lb/ft^2)	0.0323	0.0466
	(oz/yd^2)	4.65	6.71
Degree of Crimp* - warp yarns	(%)	3.1	1.1
* Elongation when straightened after removal from fabric			

Table 2 shows a matrix of the test parameters and results, including tests on both the 1.5- and 4-in. swaths for Kevlar and Zylon. In addition to testing different materials, tests were performed to compare the response of different mesh densities for Zylon (30x30, 35x35, and 40x40) and the difference for fabrics gripped on the fill and warp yarns.

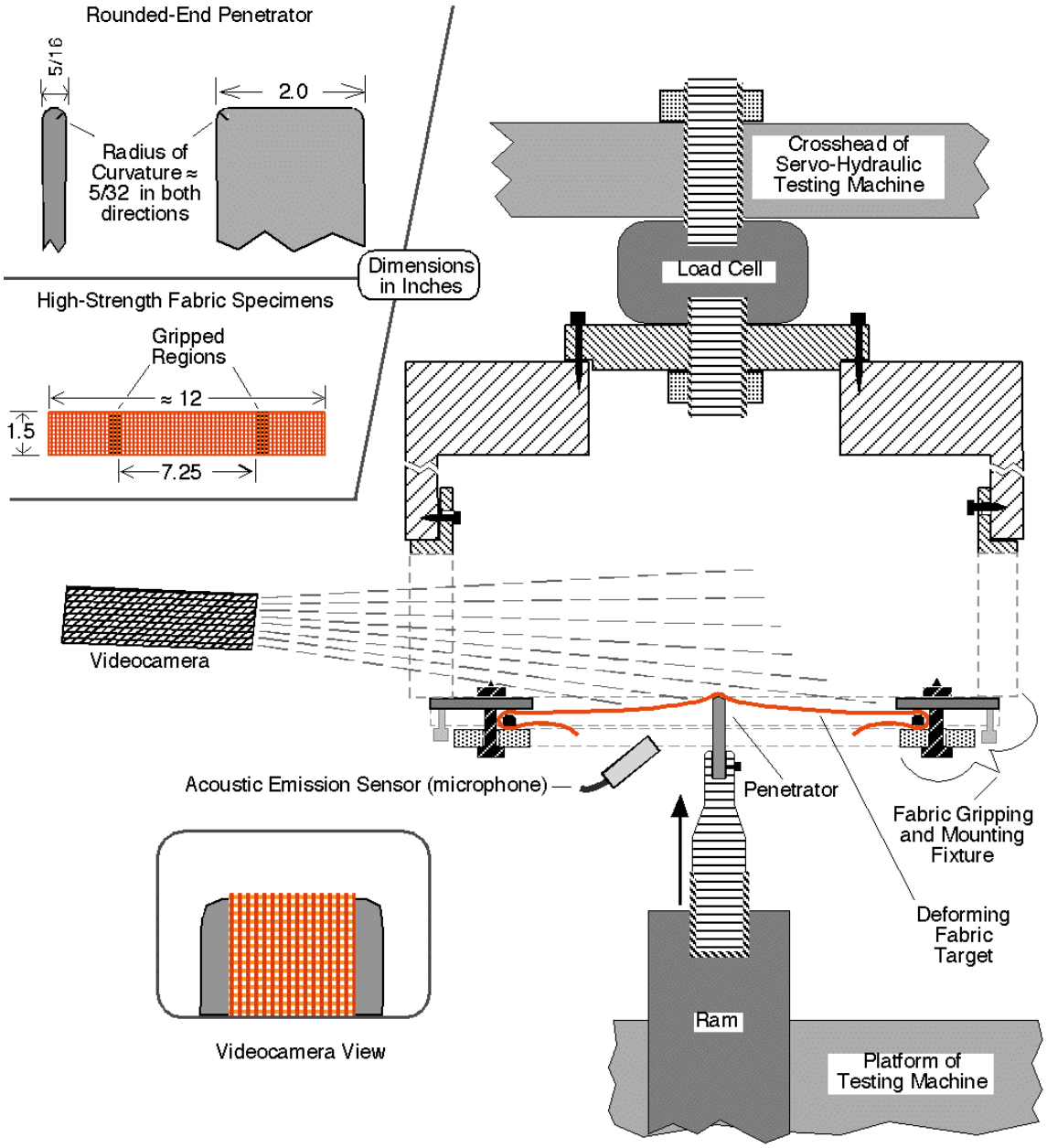

Figure 3. Experimental configuration for push tests of fabric swaths

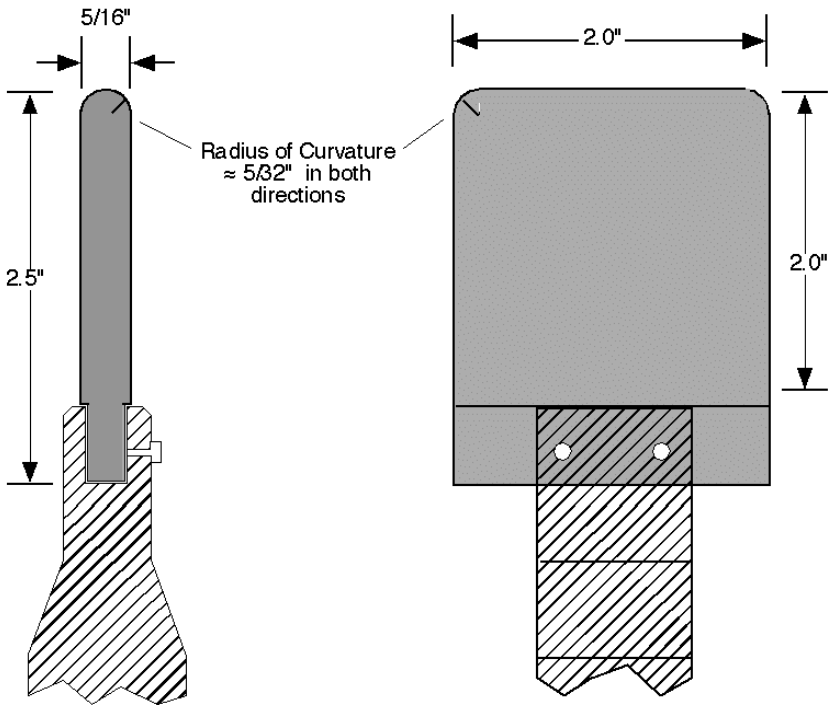

Figure 4. Penetrator geometry

Table 2. Parameters and results for push tests

PARAMETERS AND RESULTS FOR QUASI-STATIC PENETRATION (PUSH) TESTS														
Test No. (H-P:)	Material	Target[a] Weave (Yarn/in.)	Direc-tion	No. Plies	Areal Density (g/cm^2)	Fabric Width (in.)	(Yarns)	Penetrator Type[b]	Stroke Rate (in./s)	Peak Load (lb)	Energy Absorbed[c] (J)	(ft-lb)	SEA[d] (J / g/cm^2)	(ft-lb / lb/ft^2)
1	Kevlar	17x17	Warp	1	0.02275	4.0	68	RE (2" wide)	0.05	912	62.0	45.7	2723	980
4	Kevlar	17x17	Warp	1	0.02275	4.0	68	RE (2" wide)	0.05	1001	69.0	50.9	3032	1092
2	Zylon	35X35	Warp	1	0.01575	4.0	140	RE (2" wide)	0.05	1417	115.4	85.1	7325	2637
3	Zylon	35X35	Warp	1	0.01575	4.0	140	RE (2" wide)	0.05	1345	121.7	89.8	7727	2782
6	Kevlar	17x17	Warp	1	0.02275	1.47	25	RE (2" wide)	0.05	530	26.3	19.4	1157	417
8	Kevlar	17x17	Warp	1	0.02275	1.47	25	RE (2" wide)	0.05	570	25.3	18.7	1113	401
7	Zylon	35X35	Warp	1	0.01575	1.43	50	RE (2" wide)	0.05	760	39.6	29.2	2517	906
10	Zylon	35X35	Warp	1	0.01575	1.43	50	RE (2" wide)	0.05	839	29.8	22.0	1891	681
12	Zylon	30x30	Fill	1	0.0130	1.50	45	H (2" wide)	0.05	566	37.3	27.5	2869	1033
13	Zylon	30x30	Fill	1	0.0130	1.50	45	H (2" wide)	0.05	551	39.9	29.4	3067	1104
16	Zylon	40x40	Warp	1	0.0185	1.50	60	H (2" wide)	0.05	933	38.8	28.6	2095	754
17	Zylon	40x40	Fill	1	0.0185	1.50	60	H (2" wide)	0.05	643	47.2	34.8	2552	919

[a] Distance between grips is 7.2 in.

[b] Rounded-end penetrator (2 in. wide, 4/16 in. thick, 5/32-in. radius of curvature in both directions) - same as one used by ASU.

[c] Equals the area under the load-deflection curve.

[d] SEA = Specific Energy Absorbed = energy absorbed divided by areal density of the target.

1.5-in.- wide Swaths

Figures 5 and 6 show the fabric load displacement curves for the 1.5-in.-wide swath push tests on Kevlar and Zylon. The reproducibility of the test results was excellent. A comparison of the results for the two materials shows that the ultimate tensile strength of Kevlar 17x17 is only about 60% of that of Zylon 35x35, and the strain to failure is also significantly less.

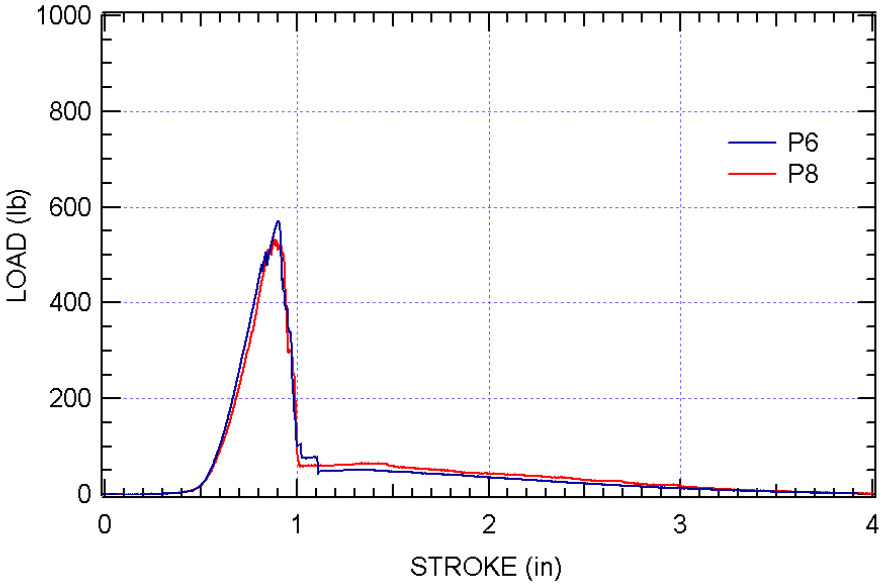

Figure 5. Kevlar push tests on 1.5 in. swaths

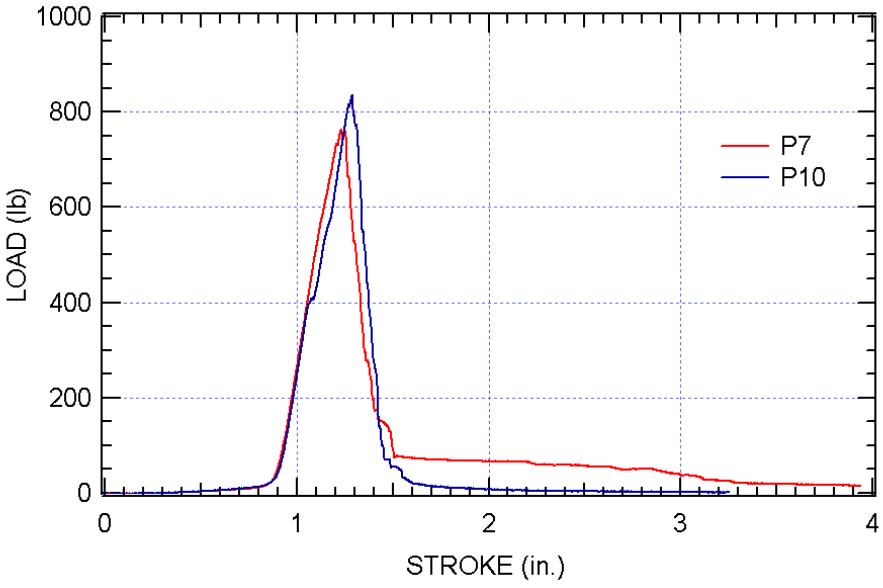

Figure 6. Zylon push tests on 1.5 in. swath

Effect of Mesh Density

To increase understanding of the fabric's deformation and failure phenomenology, we performed tests on Zylon fabrics of different mesh densities with 500 denier yarns (Zylon 30x30, 35x35 and 40x40), including fabric gripped in the fill and warp directions. Results of these tests confirmed the importance that crimp in the gripped yarns have on the resulting stress-strain curves.

The results of these tests are shown in Figures 7 and 8. Figure 7 shows the results of ram load-deflection and Figure 8 shows the calculated stress-strain curves. Note the large difference in the stroke at the first rise in load and in the stroke at the peak load for the different tests. The 40x40 warp yarns have a much larger degree of crimp (5.2% increase in length when straightened) than the 35x35 warp yarns (2.0%) or the fill yarns of either mesh (0.6% crimp). The straightening of the crimp likely accounts for the longer flat region prior to the rise. Also notice the large effect that crimp has on the load-stroke curve. Although the peak stress on the 40x40 warp yarn is significantly less than for the 40x40 fill yarns (Figure 8), because of the large amount of crimp the measured load (Figure 7) for the warp yarn is significantly greater than for the fill yarn.

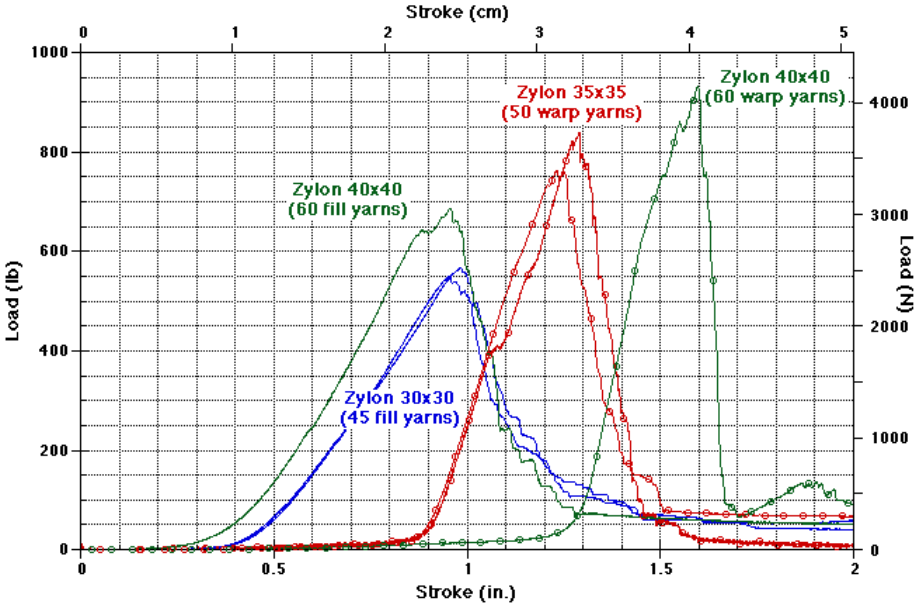

Figure 7. Effect of mesh density on push test load-stroke results

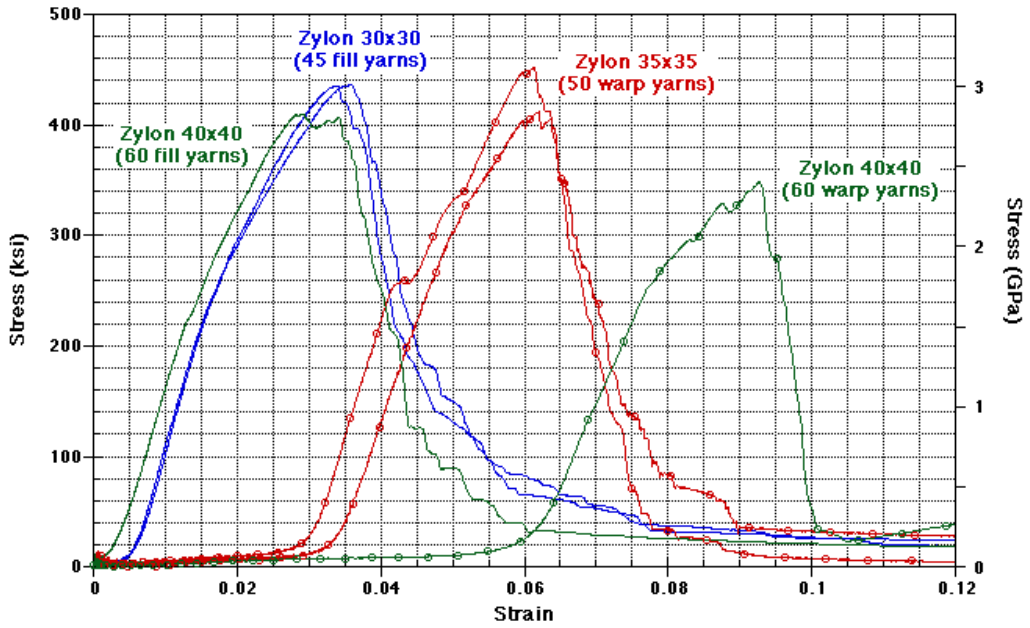

Figure 8. Nominal Zylon stress-stress curves for different mesh density swaths.

4-in.-wide Swath Tests

Results of the tests on 4-in.-swaths of Kevlar and Zylon are shown in Figures 9 and 10. Peak loads for the 4-in.-wide fabrics are much higher than for the 1.5-in.-wide swaths. More significantly, very large energies are absorbed (areas under the load-deflection curves) after the initial peak, particularly for Zylon. As listed in Table 2, note the difference in the energy absorbed for Zylon as compared to Kevlar, particularly for the 4-in-wide tests, and the even larger difference in the Specific Energy Absorbed (SEA), which is the energy absorbed divided by the fabric's areal density. (The areal density of the Kevlar fabric is about 50% higher than that of Zylon).

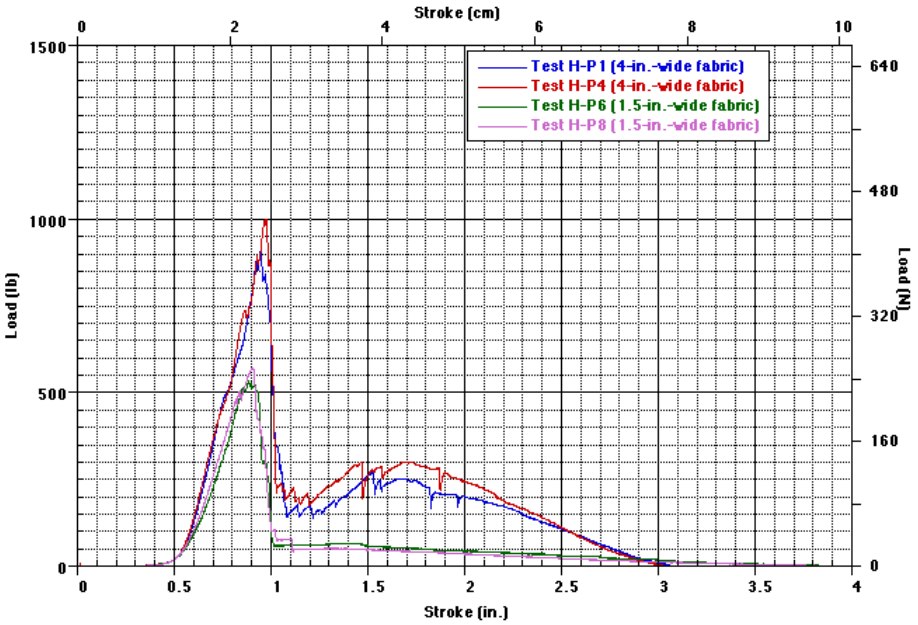

Figure 9. Kevlar push tests on 4 in. swaths

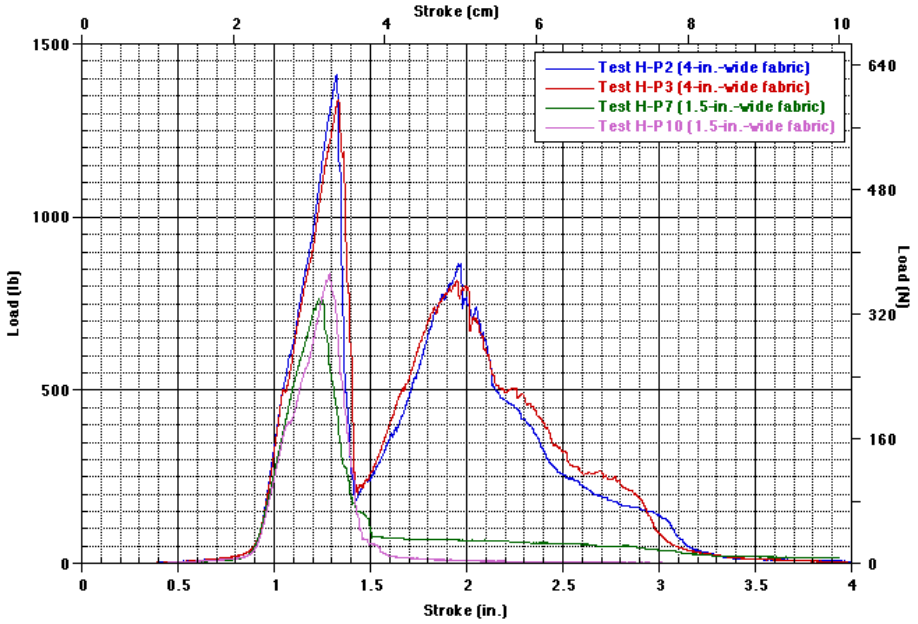

Figure 10. Zylon push tests on 4 in. swaths

Analysis of Swath Tests

Preliminary comparisons of SRI's static test results on 1.5-in. swaths with results from ASU's direct tension tests of fabric swaths results showed marked differences in the strength and stiffness of the fabrics tested. The main source of the difference was determined to be the procedure for calculating the cross-sectional area of the yarns. SRI provided ASU with an explanation of the process for converting load-deflection data to

stress-strain data for transverse loading tests and also the procedure to determine the cross-sectional area of the yarns for calculating stress from force.

Determining stress and strain for swath tests

The method for calculating stresses and strains in the fabric from load and deflection on the ram is simply a function of geometry as shown in Figure 11. This procedure is only applicable to the 1.5-in.-wide swath tests, in which all of the gripped yarns are in direct contact with the penetrator and undergo the same loading geometry.

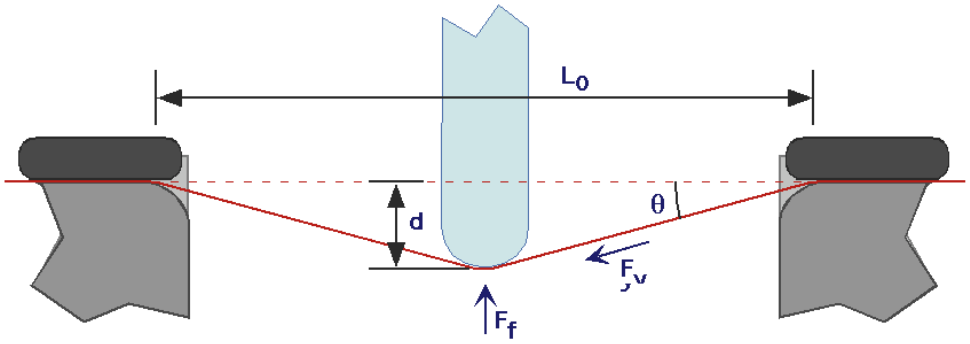

Histories of the ram displacement (d) and the vertical force on the fragment (Ff) were recorded during the test. From these histories, the axial force along the yarn (Fy) and yarn elongation (ΔL) were determined as follows (refer to above Figure):

$$F_y = \frac{F_f}{2 \sin \theta} \qquad (1)$$

where F_y = Axial Force along Yarn, θ = Arctan $(2d/L_0)$, and L_o = distance between grips

$$\Delta L = 2 [d^2 + (L_o/2)^2]^{1/2} - L_o = 2d/\sin(\theta) - L_o \qquad (2)$$

Stress is obtained by dividing the force along the yarn (F_y) by the yarn's cross-sectional area.

Strain is obtained by dividing (ΔL) the yarn elongation by the gage length (L_o).

Figure 11. Analysis of push test data.

Determining cross-sectional area of yarns

The method SRI used to determine the cross-sectional area of a yarn removed from the fabric was to: (1) measure the yarn length and mass to determine linear density. This measurement is easy to make with an accurate analytic balance. (2) Divide the linear density by the bulk material density (as obtained from the manufacturers) to obtain a cross-sectional area. The cross-sectional areas for the various yarns using this method are shown in Table 1.

The Zylon had a measured linear density of 0.556 mg/cm (exactly equal to the nominal 500 denier), which when divided by the 1.54 g/cm^3 bulk density yields a cross-sectional area of 3.61x10^{-4} sq. cm, or 5.59x10^{-5} sq. in. per yarn.

The Kevlar had a measured a linear density of 1.656 mg/cm (equal to 1590 denier, 5% higher than the nominal 1420 denier), which when divided by the 1.44 g/cm^3 bulk density, yields a cross-sectional area of 1.15x10^{-3} cm^2, or 1.78x10^{-4} in^2. per yarn.

Fabric reference web sites

As a result of discussions on determining cross-sectional areas for yarns, SRI located an informative set of web sites that give definitions and descriptions of many terms used in discussing fabrics. The first defines cotton counts and other yarn sizing parameters: http://www.sonic.net/~garyh/yarns/sizing.html. A related site gives some useful basic yarn definitions: http://www.sonic.net/~garyh/yarns/propert.html.

Cotton count is a measure of length per unit mass. This is inverse to Denier or decitex which are measures of mass per unit length or linear density. However, neither of these measures alone can be used to determine cross-sectional area (CSA), because a 1-to-1 correspondence between CSA and either cotton count or denier does not exist.

Gluing of Zylon

In planning for the static tests at ASU, we addressed the question of how to secure the ends for fabric rings, particularly for only a few plies of fabric. Both clamping and gluing were considered as alternative strategies.

SRI inquired of Toyobo, the Zylon manufacturer, whether they were aware of some adhesive for attaching Zylon to itself. We explained that we are considering a splice joint in which two ends of fabric are overlapped. We also asked if it was necessary to remove any coatings or sizings from the yarns.

Toyobo advised that gluing Zylon was difficult. The adhesion of Zylon fiber is lower than carbon fiber. Toyobo had no applicable experience in gluing Zylon, but they suggested increasing the overlap length of the fabric ends and recommended trying various glues and advised that we may get better adhesion after cleaning the surface using organic solvents such as alcohol and hexane to promote adhesion.

MEETINGSSRI personnel participated in the three project meetings held at ASU on this program including the kick-off meeting on September 5, 2001, the first review meeting held October 23, 2001, and the second review meeting held January 28, 2002.

Appendix 1. User's Manual for SRI Zylon Fabric

User-Defined Material Type 47 (Ballistic Fabric)

Columns		Quantity		
Format				
1-10	Card 3	Tensile modulus, E	E10.0	
11-20		Bidirectional failure strain, ε_{min}		E10.0
21-30		Unidirectional failure strain, ε_{max}		E10.0
31-40		Yield stress, σ_y		E10.0
41-50		Slack strain, ε_{sl}		E10.0
1-10	Card 4	Compression factor, f_{co}	(default 0.02)	
E10.0				
11-20		Shear modulus,	(default 0.02*E)	E10.0
21-30		Hardening factor , h	(default = 0.02)	E10.0
31-40		Residual strength factor, f_{co}	(default 0.20)	E10.0
41-50		Failure strain interval, ε_f	(default 0.10)	E10.0
61-70		Max. failure increment, d_{max}	(default 0.01)	E10.0

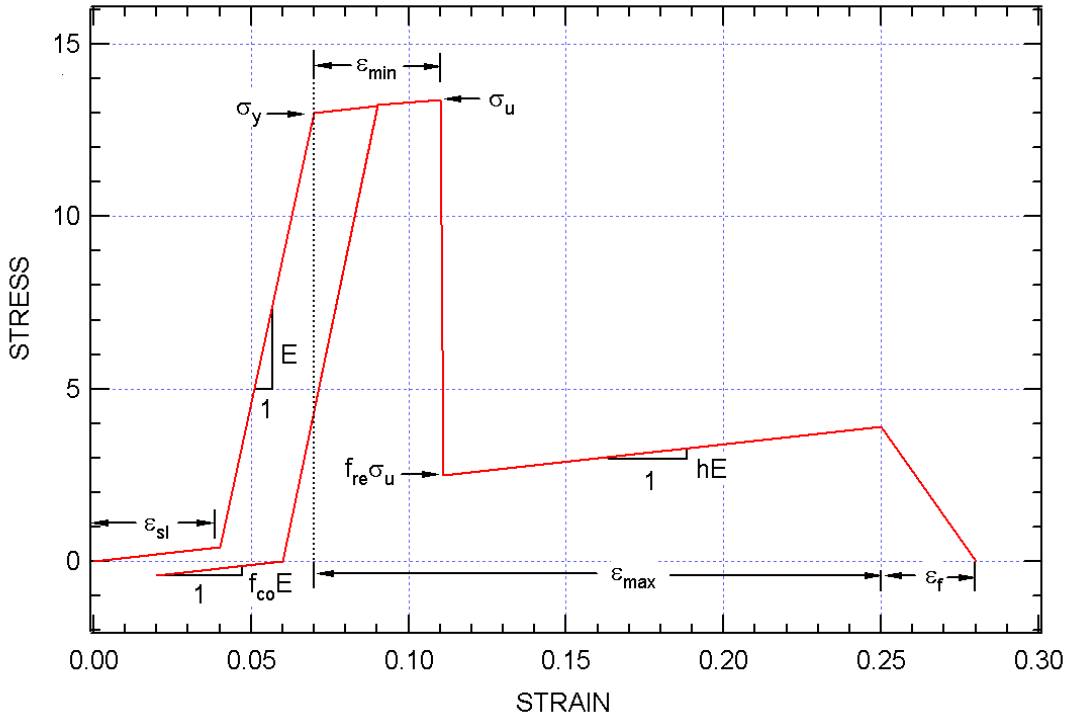

Figure 12. Uniaxial stress-strain curve for ballistic fabric model.

The ballistic fabric model is orthotropic with stress-strain response as shown in Figure 1 for each of the two yarn (local X and Y) directions. The stress-strain responses in the two directions are uncoupled, but the failure response is coupled.

$\sigma_{xx} = f(\varepsilon_{xx})$

$\sigma_{yy} = f(\varepsilon_{yy})$

$\sigma_{zz} = 0$

$\tau_{xy} = G\,\varepsilon_{xy}$

$\tau_{yz} = G\,\varepsilon_{yz}$

$\tau_{zx} = G\,\varepsilon_{zx}$

As shown in Figure 1, the uniaxial response has the following features:

- Elastic response with modulus E up to yield stress, σ_y
- Linear hardening with modulus =hE
- Elastic unloading with reduced compression modulus = f_{co} E
- Slack before straightening, prestraighted modulus = compression modulus

- Default shear modulus is small = 0.02*E
- Failure:

If plastic strain reaches ε_{min} in one direction, the strength drops to a fraction of the stress at ε_{min}

If plastic strain in both directions reaches ε_{min}, the element is failed

If plastic strain in a single direction reaches ε_{max} the element is failed